Autonomous Mapping of Underwater Objects With the Sum–Product Algorithm

DOMENICO GAGLIONE
GIOVANNI SOLDI
PAOLO BRACA

Mapping of underwater objects is usually conducted with autonomous underwater vehicles (AUVs). A standard approach in mine countermeasure (MCM) operations is to perform a two-phase reconnaissance: in the first phase, a survey mission is carried out to detect and classify the objects; in the second phase, objects are reacquired to confirm the actual presence of mines. The data acquired during this multiphase mission greatly depends on the accuracy of the AUV's navigation system. This paper proposes a graph-based mapping algorithm that takes into account the unknown AUV position, as well as the output of the classification process, and uses the sum–product algorithm (SPA) to obtain a principled and intuitive approximation of the Bayesian inference needed for object detection and estimation. The SPA-based mapping algorithm is derived in detail, and its performance is evaluated in a simulated MCM scenario.

D. Gaglione, G. Soldi, and P. Braca are with the NATO Centre for Maritime Research and Experimentation (CMRE), 19126 La Spezia, Italy (e-mail: domenico.gaglione@cmre.nato.int, giovanni.soldi@cmre.nato.int, paolo.braca@cmre.nato.int).

I. INTRODUCTION

Underwater mapping and surveying arise in a variety of applications, from environmental assessments and inspections [1]–[3] to marine archaeology [4] and mine countermeasure (MCM) operations [5].

These tasks are generally conducted with unmanned underwater vehicles, such as remotely operated vehicles (ROVs) and autonomous underwater vehicles (AUVs) [6]. ROVs are connected to a support ship or marine platform and are operated from above the water's surface. The cable provides power and high-speed communications, allowing the operator to guide the vehicle while receiving sensor data in quasi-real time. Even though the cable can extend over several kilometers, this can limit the maximum range of operations. AUVs, instead, are untethered and preprogrammed to perform a specific task with little or no operator interaction, and they are usually designed for long-range, high-endurance missions.

When performing mapping and surveying with AUVs, navigation information is of paramount importance. Indeed, the quality and value of the data acquired during a mission greatly depend on the accuracy of the vehicle's navigation system. The unavailability of global positioning system (GPS) technologies in the underwater environment, limited by the heavy attenuation of radio frequency signals, requires the use of other methods for vehicle localization, e.g., acoustic or inertial navigation [7]. Acoustic navigation is based on the use of external references (i.e., acoustic beacons) at known positions that provide navigation aids to the unmanned vehicle, such as relative range and bearing; however, the deployment of such acoustic beacons might be inconvenient or even unfeasible in some scenarios. Inertial navigation systems (INSs), instead, calculate the instantaneous position and orientation of the vehicle using high-frequency data from an inertial measurement unit (IMU) available on board. A typical IMU includes accelerometers and gyroscopes, and the INS provides position and orientation information by integrating the values measured by these devices. However, because of this integration, the inherent errors in the accelerometers and gyroscopes accumulate over time, resulting in position and orientation errors that increase over time [8], [9]. A performance measure for an INS is given by the inertial drift rate in position that, for current high-quality commercial INSs, is of several kilometers per hour [6]. Advanced techniques, e.g., aiding the INS with a Doppler velocity log, a pressure sensor, and magnetometers, can reduce this drift to less than 0.5% of the AUV's traveled distance [10].

The use of AUVs is widely acknowledged as beneficial in MCM scenarios since they allow to operate from a distance in safe conditions. A classic approach to mine-hunting is to perform a two-phase reconnaissance. During the first phase, a survey mission is carried out using an AUV equipped with a synthetic aperture sonar

(SAS) capable of detecting and classifying mine-like objects (MLOs); the AUV generally follows a *lawnmower* pattern so as to ensure full coverage of the designed area, and the classification is performed by means of automatic target recognition (ATR) techniques [11], [12]. Once potential MLOs are located, the second phase is committed to the reacquisition of the contacts with an AUV equipped with a lower-range but higher-resolution sensor [13]. This second phase is more effective as the position uncertainty of the objects detected during the first phase is limited and their classification is accurate. Therefore, the algorithm responsible for building a comprehensive map of the underwater objects—both MLOs and non-MLOs—needs to account for the inherent uncertainty of the AUV position, as well as process the ATR classification output.

The mapping algorithm can exploit the position of the detected objects to sequentially refine the estimate of the AUV position, particularly when the same area happens to be surveyed multiple times. This approach is known in the robotics literature as simultaneous localization and mapping (SLAM), and has been applied also in the underwater domain. However, due to the lack of underwater features suitable as anchor points, underwater robotic mapping has primarily been focused on structured, man-made, or confined underwater environments [14], [15]. Recently, a probability hypothesis density (PHD)-based underwater mapping algorithm has been proposed [16], [17]. The PHD filter is an example of set-type tracking algorithm in which object states and measurements are represented by random finite sets (RFSs), a formulation that is particularly convenient for addressing situations with a varying number of objects to locate, object (dis)appearance and spawning, the presence of clutter and association uncertainty, false alarms, and missed detections. However, the methods in [16], [17] do not account for the uncertain AUV position. Nevertheless, RFS-based approaches that jointly estimate the AUV position and the (mobile) object states have been presented for other applications, such as autonomous driving [18].

This paper proposes and describes a Bayesian mapping algorithm based on an emerging approach to information fusion. This approach relies on a factor graph representation of the statistical model of the underwater mapping problem—including the uncertain AUV position—and on the sum–product algorithm (SPA) to efficiently obtain a principled and intuitive approximation of the Bayesian inference needed for object detection and estimation [19], [20]. Parts of this work were presented in our conference publication [21]. This paper differs from that publication in that it extends the formulation to account for the unknown AUV position; it presents detailed derivations of the joint posterior distribution; and it presents the SPA messages in a complete and detailed manner. Note that the statistical formulation and the factor graph described in this paper are similar to those presented in [22] for multipath-based in-

door SLAM and in [23] for cooperative localization and tracking using a network of sensing agents. The main difference between the current work and those cited papers is in the application: specifically, when conducting underwater mapping with an SAS sensor, not all the objects are observable at all times. Moreover, the statistical formulation herein presented integrates the output of the ATR, enabling discrimination among different object types.

The remainder of this article is organized as follows. The basic notation and nomenclature are described in the next subsection. Section II describes the problem at hand and outlines the system model. The stochastic formulation is given in Section III, while the proposed method is detailed in Section IV. Results obtained in a simulated MCM scenario are shown in Section V, and Section VI concludes the paper.

A. Notation

Throughout this paper, column vectors are denoted by boldface lower-case letters (e.g., $\boldsymbol{a}$) and matrices by boldface upper-case letters (e.g., $\boldsymbol{A}$). $\mathbf{I}$ denotes the identity matrix and $\mathbf{1}$ denotes the column vector of all ones, with the size determined by the subscript or from the context. The transpose of a matrix $\boldsymbol{A}$ is written as $\boldsymbol{A}^{\mathrm{T}}$. We write $\mathrm{diag}(a_1, \ldots, a_n)$ for an $n \times n$ diagonal matrix with diagonal entries $a_1, \ldots, a_n$. Moreover, given a sequence $\boldsymbol{a}_1, \ldots, \boldsymbol{a}_n$, the column vector stacking all the elements of the sequence is denoted as $\boldsymbol{a}_{1:n} = [\boldsymbol{a}_1^{\mathrm{T}}, \ldots, \boldsymbol{a}_n^{\mathrm{T}}]^{\mathrm{T}}$. The Euclidean norm of vector $\boldsymbol{a}$ is denoted by $\|\boldsymbol{a}\|$. For a two-dimensional (2D) vector $\boldsymbol{a}$, $\angle \boldsymbol{a}$ is the angle defined counterclockwise and such that $\angle \boldsymbol{a} = 0$ for $\boldsymbol{a} = [1, 0]^{\mathrm{T}}$. The symbol $\propto$ denotes equality up to a constant factor. Sets are denoted by calligraphic letters (e.g., $\mathcal{A}$), the Dirac delta function is denoted by $\delta(\cdot)$, and the Kronecker delta is denoted by $\delta_{a,b}$, and is equal to 1 if $a = b$, and 0 otherwise. Finally, we denote the probability mass function (pmf) of a discrete random variable or vector by $p(\cdot)$ and the probability density function (pdf) of a continuous random variable or vector by $f(\cdot)$; the latter notation will also be used for a mixed pdf/pmf of both continuous and discrete random variables or vectors.

II. PROBLEM DESCRIPTION AND SYSTEM MODEL

A. AUV State, Navigation Data, and ATR Detections

Let $\boldsymbol{s}_t$ represent the AUV state at time step $t = 1, 2, \ldots$, whose evolution is given by the following kinematic model:

$$\boldsymbol{s}_t = \boldsymbol{\varepsilon}(\boldsymbol{s}_{t-1}, \boldsymbol{u}_t), \tag{1}$$

where $\boldsymbol{u}_t$ is a driving process noise independent across t. The AUV is equipped with an on-board device, e.g., an INS, that provides at time t a noisy observation of the AUV state $\boldsymbol{s}_t$; this observation, referred to as navigation
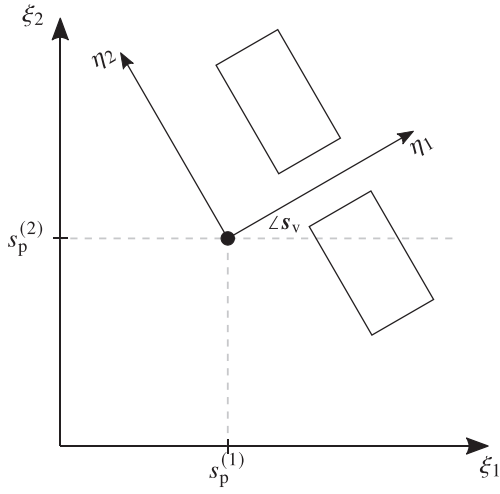
Figure 1. Illustration of the scenario (note that the time index t is omitted). The global coordinate system is (ξ_1, ξ_2). The position of the AUV (black dot) is $\boldsymbol{s}_{\mathrm{p}} = [s_{\mathrm{p}}^{(1)}, s_{\mathrm{p}}^{(2)}]^{\mathrm{T}}$, and its forward direction is given by the angle $\angle \boldsymbol{s}_{\mathrm{v}}$. The local coordinate system (η_1, η_2) is defined by the position and heading of the AUV.
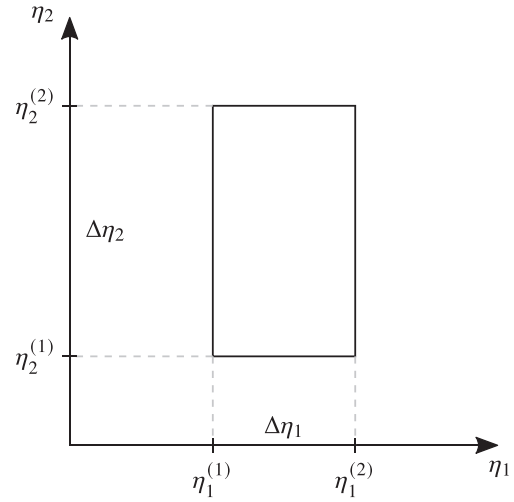

Figure 2. Geometry of the port side SAS tile in local coordinates: $(\eta_1^{(1)}, \eta_2^{(1)})$ is the location of the corner of the tile closest to the origin, i.e., the position of the AUV; $\Delta\eta_1 = \eta_1^{(2)} - \eta_1^{(1)}$ is the tile extent along η_1; $\Delta\eta_2 = \eta_2^{(2)} - \eta_2^{(1)}$ is the tile extent along η_2.

data, is modeled as

$$\boldsymbol{g}_t = \boldsymbol{\gamma}_{\mathrm{A}}(\boldsymbol{s}_t, \boldsymbol{v}_t), \tag{2}$$

where $\boldsymbol{v}_t$ is an observation process noise independent across t. To facilitate the description that follows, we consider the state $\boldsymbol{s}_t$ to be composed of the AUV's position $\boldsymbol{s}_{t,\mathrm{p}}$ and velocity $\boldsymbol{s}_{t,\mathrm{v}}$ in Cartesian coordinate, i.e., $\boldsymbol{s}_t = [\boldsymbol{s}_{t,\mathrm{p}}^{\mathrm{T}}, \boldsymbol{s}_{t,\mathrm{v}}^{\mathrm{T}}]^{\mathrm{T}}$. Nevertheless, the derivation of the proposed algorithm is general enough to accommodate a different definition of $\boldsymbol{s}_t$ that may also include additional kinematic parameters, e.g., the AUV turn rate. As illustrated in Fig. 1, the state $\boldsymbol{s}_t$ defines the AUV local coordinate system (η_1, η_2), whose origin is $\boldsymbol{s}_{t,\mathrm{p}}$ and that is rotated of an angle $\angle \boldsymbol{s}_{t,\mathrm{v}}$ in a counterclockwise direction with respect to the global coordinate system (ξ_1, ξ_2). Note that a generic point $\boldsymbol{\rho}_\xi$ in global coordinates can be converted into local coordinates as $\boldsymbol{\rho}_\eta = \boldsymbol{\theta}(\boldsymbol{\rho}_\xi; \boldsymbol{s}_t) \triangleq \boldsymbol{R}(\angle \boldsymbol{s}_{t,\mathrm{v}})[\boldsymbol{\rho}_\xi - \boldsymbol{s}_{t,\mathrm{p}}]$, where $\boldsymbol{R}(\cdot)$ is a clockwise rotation matrix.

The AUV is equipped with an SAS, a high-resolution sonar that generates acoustic images of the bottom. Such images—or SAS tiles—come in pairs, covering both port and starboard sides of the AUV, but having a coverage gap beneath. Figure 2 shows the geometry of the port side SAS tile in local coordinates (the starboard side tile is obtained by mirroring the port side tile on the η_1-axis). The SAS images are processed by an ATR algorithm that detects and classifies the features of interest, providing the location within the tile (i.e., in local coordinates) of each detection and the probabilities of such detection of being generated by an object of class $c \in \{1, \ldots, C\}$, where C is the total number of classes. Specifically, the number of detections (or measurements) extracted by the ATR algorithm from the SAS tiles at time t is m_t. The location of the mth measurement in local coordinates is represented by the vector $\boldsymbol{\ell}_{m,t} = [\ell_{m,t}^{(1)}, \ell_{m,t}^{(2)}]^{\mathrm{T}}$. The proba-

bility of the mth measurement of being generated by an object of class $c \in \{1, \ldots, C\}$ is referred to as $\pi_{m,t}^{(c)}$, and the sum of these probabilities is 1, i.e., $\sum_{j=1}^{C} \pi_{m,t}^{(j)} = 1$. Since any one of these C probabilities can be derived from the other $C - 1$, the ATR algorithm actually provides the vector $\boldsymbol{\pi}_{m,t} \triangleq [\pi_{m,t}^{(1)}, \ldots, \pi_{m,t}^{(C-1)}]^{\mathrm{T}}$, i.e., the vector stacking all the probabilities but $\pi_{m,t}^{(C)}$. Indeed, $\pi_{m,t}^{(C)}$ can then be calculated from $\boldsymbol{\pi}_{m,t}$ as $\pi_{m,t}^{(C)} = 1 - \mathbf{1}_{C-1}^{\mathrm{T}} \boldsymbol{\pi}_{m,t}$. Concretely, if the ATR algorithm distinguished between MLOs and non-MLOs, then $C = 2$, and $\pi_{m,t}^{(1)}$ and $\pi_{m,t}^{(2)} = 1 - \pi_{m,t}^{(1)}$ would be, respectively, the probability that the mth measurement is generated by an MLO, and the probability that the mth measurement is generated by a non-MLO. Unlike the approaches presented in [24], [25], here the ATR algorithm does not distinguish between object- and clutter-generated measurements. For convenience, we define the vector of the mth measurement at time t as $\boldsymbol{z}_{m,t} \triangleq [\boldsymbol{\ell}_{m,t}^{\mathrm{T}}, \boldsymbol{\pi}_{m,t}^{\mathrm{T}}]^{\mathrm{T}}$, and the vector of all the measurements extracted at time t as $\boldsymbol{z}_t \triangleq [\boldsymbol{z}_{1,t}^{\mathrm{T}}, \ldots, \boldsymbol{z}_{m_t,t}^{\mathrm{T}}]^{\mathrm{T}}$.

B. Potential Object States

As done in [23], [26], we account for a time-varying unknown number of objects by introducing the concept of *potential object* (PO). The number of POs at time t is k_t; the existence of PO $k \in \{1, \ldots, k_t\}$ at time t is indicated by the binary variable $r_{k,t} \in \{0, 1\}$, i.e., $r_{k,t} = 1$ if the PO exists and $r_{k,t} = 0$ otherwise. Position and class of PO k are denoted by $\boldsymbol{x}_{k,t}$ and $\tau_{k,t}$, respectively, and are formally considered also if $r_{k,t} = 0$. We combine the position, class, and existence variables of PO k into the state vector $\boldsymbol{y}_{k,t} \triangleq [\boldsymbol{x}_{k,t}^{\mathrm{T}}, \tau_{k,t}, r_{k,t}]^{\mathrm{T}}$, and define the joint vector of all the POs at time t as $\boldsymbol{y}_t \triangleq [\boldsymbol{y}_{1,t}^{\mathrm{T}}, \ldots, \boldsymbol{y}_{k_t,t}^{\mathrm{T}}]^{\mathrm{T}}$. We observe that the position $\boldsymbol{x}_{k,t}$ and class $\tau_{k,t}$ of any

nonexisting PO (i.e., for which $r_{k,t} = 0$) are obviously irrelevant; thus, all the pdfs defined for the PO states, i.e., $f(\underline{y}_{k,t}) = f(\underline{x}_{k,t}, \underline{\tau}_{k,t}, \underline{r}_{k,t})$, are such that

$$f(\underline{x}_{k,t}, \underline{\tau}_{k,t}, \underline{r}_{k,t} = 0) = f_{k,t}\, f_{\mathrm{D}}(\underline{x}_{k,t}, \underline{\tau}_{k,t}),$$

where $f_{k,t} \in [0, 1]$ is a constant and $f_{\mathrm{D}}(\underline{x}_{k,t}, \underline{\tau}_{k,t})$ is an arbitrary *dummy* pdf.

Each PO at time t is either a *new* PO or a *legacy* PO. New POs model those objects that are detected for the first time by the ATR algorithm at time t. Each new PO corresponds to a measurement $z_{m,t}$; therefore, the number of new POs at time t is m_t. The state of a new PO is denoted by $\bar{y}_{m,t} \triangleq [\bar{x}_{m,t}^{\mathrm{T}}, \bar{\tau}_{m,t}, \bar{r}_{m,t}]^{\mathrm{T}}, m \in \{1, \ldots, m_t\}$, and $\bar{r}_{m,t} = 1$ thus means that measurement m was generated by an object that was never detected before, namely, a *newly detected* object; we define the joint state vector of all new POs introduced at time t as $\bar{y}_t \triangleq [\bar{y}_{1,t}^{\mathrm{T}}, \ldots, \bar{y}_{m_t,t}^{\mathrm{T}}]^{\mathrm{T}}$. A legacy PO is a PO that has already been introduced at any previous time $t' < t$. We indicate with $\underline{y}_{k,t} \triangleq [\underline{x}_{k,t}^{\mathrm{T}}, \underline{\tau}_{k,t}, \underline{r}_{k,t}]^{\mathrm{T}}$ the state of legacy PO $k \in \{1, \ldots, k_{t-1}\}$, and with $\underline{y}_t \triangleq [\underline{y}_{1,t}^{\mathrm{T}}, \ldots, \underline{y}_{k_{t-1},t}^{\mathrm{T}}]^{\mathrm{T}}$ the joint legacy PO state vector. The k_{t-1} legacy POs and the m_t new POs form the set of $k_t = k_{t-1} + m_t$ POs at time t, i.e., $y_t \triangleq [\underline{y}_t^{\mathrm{T}}, \bar{y}_t^{\mathrm{T}}]$, which will then become legacy POs at time $t + 1$. Note that using this mechanism, the number of POs grows indefinitely over time. To keep a tractable number of POs, a suboptimal pruning step is performed once all the measurements at time t are processed; details are provided in Section IV-F.

The joint PO state y_t evolves over time according to a first-order Markov model, and each PO state vector $y_{k,t}$ evolves independently [23], [26]. Moreover, recalling that for each PO at time $t - 1$, there is one legacy PO at time t, the joint PO state transition pdf is

$$f(\underline{y}_t | y_{t-1}) = \prod_{k=1}^{k_{t-1}} f(\underline{y}_{k,t} | y_{k,t-1}). \tag{3}$$

Note that the number of POs at time $t = 0$ is zero, i.e., $k_0 = 0$; therefore, for $t = 1$, the transition pdf in (3) is the result of an empty product, that is, $f(\underline{y}_1 | y_0) = 1$. Furthermore, assuming that given the position and existence of PO k at time $t - 1$ (i.e., $x_{k,t-1}$ and $r_{k,t-1}$), the position and existence of legacy PO k at time t (i.e., $\underline{x}_{k,t}$ and $\underline{r}_{k,t}$) are conditionally independent of the PO class at time $t - 1$ and the legacy PO class at time t (i.e., $\tau_{k,t-1}$ and $\underline{\tau}_{k,t}$); and that given $\tau_{k,t-1}$, the legacy PO class $\underline{\tau}_{k,t}$ is conditionally independent of $x_{k,t-1}$ and $r_{k,t-1}$, we obtain

$$
\begin{aligned}
f(\underline{y}_{k,t} | y_{k,t-1}) &= f(\underline{x}_{k,t}, \underline{\tau}_{k,t}, \underline{r}_{k,t} | x_{k,t-1}, \tau_{k,t-1}, r_{k,t-1}) \\
&= f(\underline{x}_{k,t}, \underline{r}_{k,t} | \underline{\tau}_{k,t}, x_{k,t-1}, \tau_{k,t-1}, r_{k,t-1}) \\
&\quad \times p(\underline{\tau}_{k,t} | x_{k,t-1}, \tau_{k,t-1}, r_{k,t-1}) \\
&= f(\underline{x}_{k,t}, \underline{r}_{k,t} | x_{k,t-1}, r_{k,t-1})\, p(\underline{\tau}_{k,t} | \tau_{k,t-1}).
\end{aligned} \tag{4}
$$

Since in the considered scenario the objects, hence the POs, are stationary (i.e., they cannot leave the surveilled area), the pdf $f(\underline{x}_{k,t}, \underline{r}_{k,t} | x_{k,t-1}, r_{k,t-1})$ is defined as follows: if PO k does not exist at time $t - 1$, i.e., if $r_{k,t-1} = 0$, then it cannot exist as legacy PO at time t; if it does exist at time $t - 1$, i.e., if $r_{k,t-1} = 1$, then it exists as legacy PO at time t and its position $\underline{x}_{k,t}$ is distributed according to the transition pdf $f(\underline{x}_{k,t} | x_{k,t-1}) = \delta(\underline{x}_{k,t} - x_{k,t-1})$, that is,

$$
\begin{aligned}
&f(\underline{x}_{k,t}, \underline{r}_{k,t} | x_{k,t-1}, r_{k,t-1}) \\
&= \begin{cases} (1 - \underline{r}_{k,t}) f_{\mathrm{D}}(\underline{x}_{k,t}), & r_{k,t-1} = 0, \\ \underline{r}_{k,t} f(\underline{x}_{k,t} | x_{k,t-1}), & r_{k,t-1} = 1, \end{cases}
\end{aligned} \tag{5}
$$

where $f_{\mathrm{D}}(\underline{x}_{k,t}) = \sum_{\underline{\tau}_{k,t}=1}^{C} f_{\mathrm{D}}(\underline{x}_{k,t}, \underline{\tau}_{k,t})$. Additionally, given that the class of an object cannot change over time, the pmf $p(\underline{\tau}_{k,t} | \tau_{k,t-1}) = \delta_{\underline{\tau}_{k,t}, \tau_{k,t-1}}$.

C. ATR Measurement Model

The probability that PO k is detected by the ATR algorithm at time t, i.e., that PO k generates a measurement $z_{m,t}$, is function of the PO position $x_{k,t}$ and class $\tau_{k,t}$, as well as of the AUV state s_t, and is denoted by $P_{\mathrm{d}}(x_{k,t}, \tau_{k,t}, s_t)$. As an example, the probability of detection could be nonzero only inside the SAS tiles, i.e.,

$$
\begin{aligned}
&P_{\mathrm{d}}(x_{k,t}, \tau_{k,t}, s_t) \\
&\triangleq \begin{cases} p_{\mathrm{d}}(\tau_{k,t}) & \text{if } \theta(x_{k,t}; s_t) \text{ is within the SAS tiles}, \\ 0 & \text{otherwise}, \end{cases}
\end{aligned}
$$

where $p_{\mathrm{d}}(\tau_{k,t})$ is a class-dependent probability of detection. Alternatively, $P_{\mathrm{d}}(x_{k,t}, \tau_{k,t}, s_t)$ could also account for some environmental characteristics, such as the bottom type [27].

The statistical dependency of a PO-generated measurement $z_{m,t}$ on the PO position $x_{k,t}$ and class $\tau_{k,t}$, and on the AUV state s_t, is described by the likelihood function $f(z_{m,t} | x_{k,t}, \tau_{k,t}, s_t) = f(\ell_{m,t}, \pi_{m,t} | x_{k,t}, \tau_{k,t}, s_t)$. Following [24] and assuming that $\ell_{m,t}$ is conditionally independent of $\pi_{m,t}$ and $\tau_{k,t}$ given $x_{k,t}$ and s_t, and that $\pi_{m,t}$ is conditionally independent of $x_{k,t}$ and s_t given $\tau_{k,t}$, the likelihood function can be factorized as

$$
\begin{aligned}
f(z_{m,t} | x_{k,t}, \tau_{k,t}, s_t) &= f(\ell_{m,t}, \pi_{m,t} | x_{k,t}, \tau_{k,t}, s_t) \\
&= f(\ell_{m,t} | \pi_{m,t}, x_{k,t}, \tau_{k,t}, s_t) f(\pi_{m,t} | x_{k,t}, \tau_{k,t}, s_t) \\
&= f(\ell_{m,t} | x_{k,t}, s_t) f(\pi_{m,t} | \tau_{k,t}).
\end{aligned} \tag{6}
$$

The first factor in (6), i.e., $f(\ell_{m,t} | x_{k,t}, s_t)$, is determined by the ATR measurement model, defined as

$$\ell_{m,t} = \gamma_{\mathrm{O}}\big(\theta(x_{k,t}; s_t), \omega_{m,t}\big),$$

and by the statistics of the ATR measurement noise $\omega_{m,t}$, assumed independent across m and t. The second factor in (6), i.e., $f(\pi_{m,t} | \tau_{k,t})$, is modeled according to a Dirichlet distribution with vector parameter $\alpha_{\tau_{k,t}} \triangleq$

$[\alpha_{\tau_{k,t}}^{(1)}, \ldots, \alpha_{\tau_{k,t}}^{(C)}]^{\mathrm{T}}$, that is,

$$f(\boldsymbol{\pi}_{m,t}|\tau_{k,t} = c) = \frac{1}{B(\boldsymbol{\alpha}_c)} \prod_{j=1}^{C-1} \pi_{m,t}^{(j)}{}^{(\alpha_c^{(j)}-1)}$$

$$\times \left(1 - \mathbf{1}_{C-1}^{\mathrm{T}} \boldsymbol{\pi}_{m,t}\right)^{(\alpha_c^{(C)}-1)}, \qquad (7)$$

where $B(\cdot)$ is the multivariate beta function.

A clutter-generated measurement (i.e., a false-alarm) is statistically described by the pdf $f_{\mathrm{FA}}(\boldsymbol{z}_{m,t}) = f_{\mathrm{FA}}(\boldsymbol{\ell}_{m,t}, \boldsymbol{\pi}_{m,t})$ that, assuming the independence between $\boldsymbol{\ell}_{m,t}$ and $\boldsymbol{\pi}_{m,t}$, can be factorized as $f_{\mathrm{FA}}(\boldsymbol{z}_{m,t}) = f_0(\boldsymbol{\ell}_{m,t})g_0(\boldsymbol{\pi}_{m,t})$. The number of clutter-generated measurements at each time t within both the port side and starboard side tiles is assumed Poisson distributed with mean μ_0.

D. Data Association

The measurements $\boldsymbol{z}_{m,t}$, $m \in \{1, \ldots, m_t\}$, have unknown origins, namely, it is unknown if a given measurement is generated from clutter or from a PO, and from which PO. Here, we consider the *point-object assumption*, stating that, at each time t, a measurement $\boldsymbol{z}_{m,t}$ originates either from a legacy PO, or from a new PO, or from clutter, and it cannot originate from more than one source (legacy POs, new POs, or clutter) simultaneously. Conversely, each PO (either legacy or new) can generate at most one measurement at time t [28]. Following [23], [26], the association between the k_{t-1} legacy POs, m_t new POs, and m_t measurements can be mathematically described by introducing: (i) the set $\mathcal{N}_t$ of measurements generated by newly detected objects at time t, that is, $\mathcal{N}_t \triangleq \{m \in \{1, \ldots, m_t\} : \bar{r}_{m,t} = 1\}$; (ii) the legacy PO-oriented association vector $\boldsymbol{a}_t \triangleq [a_{1,t}, \ldots, a_{k_{t-1},t}]^{\mathrm{T}}$; and (iii) the measurement-oriented association vector $\boldsymbol{b}_t \triangleq [b_{1,t}, \ldots, b_{m_t,t}]^{\mathrm{T}}$. Specifically, $a_{k,t}$ is defined as $m \in \{1, \ldots, m_t\}$ if legacy PO k generates measurement m, and as 0 if legacy PO k does not generate any measurement. Similarly, $b_{m,t}$ is defined as $k \in \{1, \ldots, k_{t-1}\}$ if measurement m originates from legacy PO k and as 0 if measurement m does not originate from any legacy PO. Note that $b_{m,t} = 0$ implies that measurement m either is clutter-generated or originates from a newly detected object. Then, the point-object assumption can be expressed by the indicator function $\Phi(\boldsymbol{a}_t, \boldsymbol{b}_t)$, defined as [23]

$$\Phi(\boldsymbol{a}_t, \boldsymbol{b}_t) \triangleq \Psi(\boldsymbol{a}_t, \boldsymbol{b}_t) \prod_{m \in \mathcal{N}_t} \Gamma(b_{m,t}), \qquad (8)$$

where

$$\Gamma(b_{m,t}) \triangleq \begin{cases} 0 & b_{m,t} \in \{1, \ldots, k_{t-1}\}, \\ 1 & b_{m,t} = 0, \end{cases} \qquad (9)$$

and

$$\Psi(\boldsymbol{a}_t, \boldsymbol{b}_t) \triangleq \prod_{k=1}^{k_{t-1}} \prod_{m=1}^{m_t} \psi(a_{k,t}, b_{m,t}), \qquad (10)$$

with

$$\psi(a_{k,t}, b_{m,t}) \triangleq \begin{cases} 0 & a_{k,t} = m \text{ and } b_{m,t} \neq k, \\ & \quad \text{or } a_{k,t} \neq m \text{ and } b_{m,t} = k, \\ 1 & \text{otherwise}. \end{cases}$$

Note that, since the product in (8) is over the set $\mathcal{N}_t$, the indicator function $\Phi(\boldsymbol{a}_t, \boldsymbol{b}_t)$ formally depends also on the new PO existence variables $\bar{r}_{m,t}, m \in \{1, \ldots, m_t\}$. Expression (8) can be easily explained as follows: valid associations described by $\boldsymbol{a}_t, \boldsymbol{b}_t$, and the new PO existence variables $\bar{r}_{m,t}, m \in \{1, \ldots, m_t\}$, are those for which $\Phi(\boldsymbol{a}_t, \boldsymbol{b}_t) = 1$; and we note that $\Psi(\boldsymbol{a}_t, \boldsymbol{b}_t)$ is 0 if a measurement is associated with two or more legacy POs (and, vice versa, if a legacy PO is associated with two or more measurements), and 1 otherwise; and that the product over $m \in \mathcal{N}_t$ of $\Gamma(b_{m,t})$ is 0 if any measurement generated by a new PO is also associated with a legacy PO, and 1 otherwise.

III. STOCHASTIC PROBLEM FORMULATION

A. Joint Posterior pdf

The objective of the mapping of underwater objects is to determine if a PO exists and estimate its position and class given all AUV navigation data and all measurements extracted by the ATR algorithm up to time t, i.e., given $\boldsymbol{g}_{1:t}$ and $\boldsymbol{z}_{1:t}$. In the Bayesian framework here described, this essentially consists in evaluating for each PO $k \in \{1, \ldots, k_t\}$ the posterior marginal pmf $p(r_{k,t}|\boldsymbol{g}_{1:t}, \boldsymbol{z}_{1:t})$, used for existence declaration,[1] and the conditional marginal pdf $f(\boldsymbol{x}_{k,t}|r_{k,t} = 1, \boldsymbol{g}_{1:t}, \boldsymbol{z}_{1:t})$ and pmf $p(\tau_{k,t}|r_{k,t} = 1, \boldsymbol{g}_{1:t}, \boldsymbol{z}_{1:t})$, used for position and class estimation, respectively. These marginal posterior distributions can be calculated by simple elementary operations—including marginalization—from the joint posterior distribution $f(\boldsymbol{y}_{0:t}, \boldsymbol{s}_{0:t}, \boldsymbol{a}_{1:t}, \boldsymbol{b}_{1:t}|\boldsymbol{g}_{1:t}, \boldsymbol{z}_{1:t}) = f(\boldsymbol{x}_{0:t}, \boldsymbol{\tau}_{0:t}, \boldsymbol{r}_{0:t}, \boldsymbol{s}_{0:t}, \boldsymbol{a}_{1:t}, \boldsymbol{b}_{1:t}|\boldsymbol{g}_{1:t}, \boldsymbol{z}_{1:t})$. Here, the sequence of AUV states $\boldsymbol{s}_{0:t}$ is considered as nuisance parameters to be marginalized out, where $\boldsymbol{s}_0$ is the state at time $t = 0$ whose prior distribution $f(\boldsymbol{s}_0)$ is known; $\boldsymbol{y}_0$ is introduced for mathematical convenience, since at time $t = 0$ the number of POs is zero, i.e., $k_0 = 0$. This joint posterior pdf can be factorized as (details are provided in the Appendix)

$$f(\boldsymbol{y}_{0:t}, \boldsymbol{s}_{0:t}, \boldsymbol{a}_{1:t}, \boldsymbol{b}_{1:t}|\boldsymbol{g}_{1:t}, \boldsymbol{z}_{1:t}) \propto f(\boldsymbol{s}_0) f(\boldsymbol{y}_0)$$

$$\times \prod_{t'=1}^{t} f(\underline{\boldsymbol{y}}_{t'}|\boldsymbol{y}_{t'-1}) f(\boldsymbol{s}_{t'}|\boldsymbol{s}_{t'-1}) f(\boldsymbol{g}_{t'}|\boldsymbol{s}_{t'})$$

$$\times f(\bar{\boldsymbol{y}}_{t'}, \boldsymbol{a}_{t'}, \boldsymbol{b}_{t'}, m_{t'}|\underline{\boldsymbol{y}}_{t'}, \boldsymbol{s}_{t'}) f(\boldsymbol{z}_{t'}|\boldsymbol{y}_{t'}, \boldsymbol{s}_{t'}, \boldsymbol{a}_{t'}, m_{t'}),$$

$$(11)$$

---

[1]The existence of PO k is confirmed if $p(r_{k,t} = 1|\boldsymbol{g}_{1:t}, \boldsymbol{z}_{1:t})$ is above an existence threshold E_{th} [29, Ch. 2].

where $f(\underline{\boldsymbol{y}}_t|\boldsymbol{y}_{t-1})$ is defined in (3), $f(\boldsymbol{s}_t|\boldsymbol{s}_{t-1})$ derives from the kinematic model in (1), and $f(\boldsymbol{g}_t|\boldsymbol{s}_t)$ is the likelihood determined by the navigation data model in (2). Following the derivations in [26], next we provide expressions for the prior data association pdf $f(\bar{\boldsymbol{y}}_t, \boldsymbol{a}_t, \boldsymbol{b}_t, m_t|\underline{\boldsymbol{y}}_t, \boldsymbol{s}_t)$ and the measurement likelihood $f(\boldsymbol{z}_t|\boldsymbol{y}_t, \boldsymbol{s}_t, \boldsymbol{a}_t, m_t)$.

B. Prior Data Association pdf

By considering the point-object assumption (cf. Section II-D), and assuming that positions and classes of legacy POs and new POs at time t are independent, the pdf $f(\bar{\boldsymbol{y}}_t, \boldsymbol{a}_t, \boldsymbol{b}_t, m_t|\underline{\boldsymbol{y}}_t, \boldsymbol{s}_t)$ can be expressed as

$$f(\bar{\boldsymbol{y}}_t, \boldsymbol{a}_t, \boldsymbol{b}_t, m_t|\underline{\boldsymbol{y}}_t, \boldsymbol{s}_t) \propto \Psi(\boldsymbol{a}_t, \boldsymbol{b}_t)$$
$$\times \prod_{k=1}^{k_{t-1}} q_1(\underline{\boldsymbol{y}}_{k,t}, a_{k,t}, \boldsymbol{s}_t; m_t) \prod_{m=1}^{m_t} h_1(\bar{\boldsymbol{y}}_{m,t}, b_{m,t}). \quad (12)$$

The derivation of this pdf closely follows the derivation of the pdf in [26, eq. (60)] and is thus omitted. The proportionality is due to a constant factor that only depends on the number of measurements m_t, the indicator function $\Psi(\boldsymbol{a}_t, \boldsymbol{b}_t)$ is defined in (10), and the functions $q_1(\cdot)$ and $h_1(\cdot)$—representing the contributions to the prior data association pdf of the legacy and new POs, respectively—are provided in the following. The function $q_1(\underline{\boldsymbol{y}}_{k,t}, a_{k,t}, \boldsymbol{s}_t; m_t) = q_1(\underline{\boldsymbol{x}}_{k,t}, \underline{\tau}_{k,t}, \underline{r}_{k,t}, a_{k,t}, \boldsymbol{s}_t; m_t)$ is defined for $\underline{r}_{k,t} = 1$ as

$$q_1(\underline{\boldsymbol{x}}_{k,t}, \underline{\tau}_{k,t}, \underline{r}_{k,t} = 1, a_{k,t}, \boldsymbol{s}_t; m_t)$$
$$\triangleq \begin{cases} \dfrac{P_{\mathrm{d}}(\underline{\boldsymbol{x}}_{k,t}, \underline{\tau}_{k,t}, \boldsymbol{s}_t)}{\mu_0} & a_{k,t} \in \{1, \dots, m_t\}, \\ 1 - P_{\mathrm{d}}(\underline{\boldsymbol{x}}_{k,t}, \underline{\tau}_{k,t}, \boldsymbol{s}_t) & a_{k,t} = 0, \end{cases}$$
$$(13)$$

and for $\underline{r}_{k,t} = 0$ as

$$q_1(\underline{\boldsymbol{x}}_{k,t}, \underline{\tau}_{k,t}, \underline{r}_{k,t} = 0, a_{k,t}, \boldsymbol{s}_t; m_t) \triangleq \delta_{a_{k,t},0}. \quad (14)$$

The function $h_1(\bar{\boldsymbol{y}}_{m,t}, b_{m,t}) = h_1(\bar{\boldsymbol{x}}_{m,t}, \bar{\tau}_{m,t}, \bar{r}_{m,t}, b_{m,t})$ is defined for $\bar{r}_{m,t} = 1$ as

$$h_1(\bar{\boldsymbol{x}}_{m,t}, \bar{\tau}_{m,t}, \bar{r}_{m,t} = 1, b_{m,t}) \triangleq \Gamma(b_{m,t}) \frac{\mu_{\mathrm{N}}}{\mu_0} f_{\mathrm{N}}(\bar{\boldsymbol{x}}_{m,t}, \bar{\tau}_{m,t})$$
$$= \begin{cases} 0 & b_{m,t} \in \{1, \dots, k_{t-1}\}, \\ \dfrac{\mu_{\mathrm{N}}}{\mu_0} f_{\mathrm{N}}(\bar{\boldsymbol{x}}_{m,t}, \bar{\tau}_{m,t}) & b_{m,t} = 0, \end{cases}$$
$$(15)$$

and for $\bar{r}_{m,t} = 0$ as

$$h_1(\bar{\boldsymbol{x}}_{m,t}, \bar{\tau}_{m,t}, \bar{r}_{m,t} = 0, b_{m,t}) \triangleq f_{\mathrm{D}}(\bar{\boldsymbol{x}}_{m,t}, \bar{\tau}_{m,t}). \quad (16)$$

Here, μ_{N} is the mean number of newly detected object at each time t (assumed Poisson distributed) and $f_{\mathrm{N}}(\bar{\boldsymbol{x}}_{m,t}, \bar{\tau}_{m,t})$ is the prior distribution of position and class of a new PO that, assuming the independence between $\bar{\boldsymbol{x}}_{m,t}$ and $\bar{\tau}_{m,t}$, can be factorized as $f_{\mathrm{N}}(\bar{\boldsymbol{x}}_{m,t}, \bar{\tau}_{m,t}) = f_{\mathrm{n}}(\bar{\boldsymbol{x}}_{m,t}) f_{\mathrm{n}}(\bar{\tau}_{m,t})$. Note that the function

$h_1(\cdot)$ incorporates the indicator function $\Gamma(\cdot)$ defined in (9), and that the combined use in (12) of the functions $\Psi(\boldsymbol{a}_t, \boldsymbol{b}_t)$ and $h_1(\cdot)$ describes the point-object assumption as done by the indicator function $\Phi(\cdot)$ defined in (8).

C. ATR Measurements Likelihood

By considering the point-object assumption (cf. Section II-D) and assuming that PO-generated measurements and clutter-generated measurements are independent, the measurement likelihood $f(\boldsymbol{z}_t|\boldsymbol{y}_t, \boldsymbol{s}_t, \boldsymbol{a}_t, m_t) = f(\boldsymbol{z}_t|\bar{\boldsymbol{y}}_t, \underline{\boldsymbol{y}}_t, \boldsymbol{s}_t, \boldsymbol{a}_t, m_t)$ can be expressed as

$$f(\boldsymbol{z}_t|\bar{\boldsymbol{y}}_t, \underline{\boldsymbol{y}}_t, \boldsymbol{s}_t, \boldsymbol{a}_t, m_t) \propto \prod_{k=1}^{k_{t-1}} q_2(\underline{\boldsymbol{y}}_{k,t}, a_{k,t}, \boldsymbol{s}_t; \boldsymbol{z}_t)$$
$$\times \prod_{m=1}^{m_t} h_2(\bar{\boldsymbol{y}}_{m,t}, \boldsymbol{s}_t; \boldsymbol{z}_{m,t}). \quad (17)$$

The derivation of the likelihood in (17) closely follows the derivation of the likelihood in [26, eq. (64)] and is thus omitted. The proportionality is due to a constant factor that only depends on the measurement vector $\boldsymbol{z}_t$, and the functions $q_2(\cdot)$ and $h_2(\cdot)$—embedding the measurement likelihoods related to the legacy and new POs, respectively—are provided in the following. The function $q_2(\underline{\boldsymbol{y}}_{k,t}, a_{k,t}, \boldsymbol{s}_t; \boldsymbol{z}_t) = q_2(\underline{\boldsymbol{x}}_{k,t}, \underline{\tau}_{k,t}, \underline{r}_{k,t}, a_{k,t}, \boldsymbol{s}_t; \boldsymbol{z}_t)$ is defined for $\underline{r}_{k,t} = 1$ as

$$q_2(\underline{\boldsymbol{x}}_{k,t}, \underline{\tau}_{k,t}, \underline{r}_{k,t} = 1, a_{k,t}, \boldsymbol{s}_t; \boldsymbol{z}_t)$$
$$\triangleq \begin{cases} \dfrac{f(\boldsymbol{z}_{m,t}|\underline{\boldsymbol{x}}_{k,t}, \underline{\tau}_{k,t}, \boldsymbol{s}_t)}{f_{\mathrm{FA}}(\boldsymbol{z}_{m,t})} & a_{k,t} \in \{1, \dots, m_t\}, \\ 1 & a_{k,t} = 0, \end{cases}$$
$$(18)$$

and for $\underline{r}_{k,t} = 0$ as

$$q_2(\underline{\boldsymbol{x}}_{k,t}, \underline{\tau}_{k,t}, \underline{r}_{k,t} = 0, a_{k,t}, \boldsymbol{s}_t; \boldsymbol{z}_t) \triangleq 1. \quad (19)$$

The function $h_2(\bar{\boldsymbol{y}}_{m,t}, \boldsymbol{s}_t; \boldsymbol{z}_{m,t}) = h_2(\bar{\boldsymbol{x}}_{m,t}, \bar{\tau}_{m,t}, \bar{r}_{m,t}, \boldsymbol{s}_t; \boldsymbol{z}_{m,t})$ is defined as

$$h_2(\bar{\boldsymbol{x}}_{m,t}, \bar{\tau}_{m,t}, \bar{r}_{m,t}, \boldsymbol{s}_t; \boldsymbol{z}_{m,t})$$
$$\triangleq \begin{cases} \dfrac{f(\boldsymbol{z}_{m,t}|\bar{\boldsymbol{x}}_{m,t}, \bar{\tau}_{m,t}, \boldsymbol{s}_t)}{f_{\mathrm{FA}}(\boldsymbol{z}_{m,t})} & \bar{r}_{m,t} = 1, \\ 1 & \bar{r}_{m,t} = 0. \end{cases}$$
$$(20)$$

IV. PROPOSED METHOD

A. Factor Graph and Message Scheduling

The final factorization of the joint posterior pdf $f(\boldsymbol{y}_{0:t}, \boldsymbol{s}_{0:t}, \boldsymbol{a}_{1:t}, \boldsymbol{b}_{1:t}|\boldsymbol{g}_{1:t}, \boldsymbol{z}_{1:t})$—obtained by inserting (10)
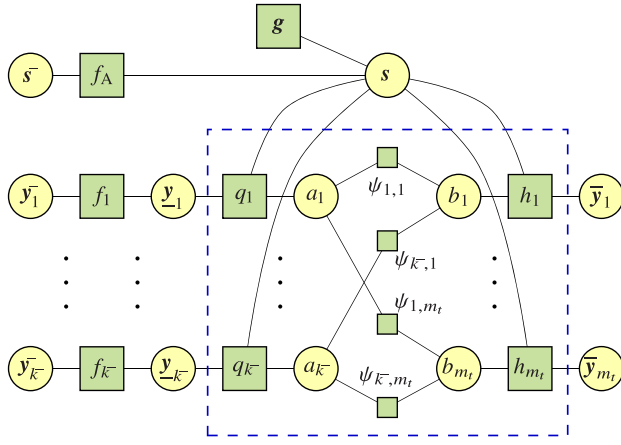
Figure 3. Factor graph representing the factorization in (21) of the joint posterior pdf $f(\mathbf{y}_{0:t}, \mathbf{s}_{0:t}, \mathbf{a}_{1:t}, \mathbf{b}_{1:t} | \mathbf{g}_{1:t}, \mathbf{z}_{1:t})$ for a single time step. Solid circles and squares represent variable nodes and factor nodes, respectively. The following short notations are used: $\bar{\mathbf{s}} \triangleq \mathbf{s}_{t-1}$; $\mathbf{s} \triangleq \mathbf{s}_t$; $\bar{\mathbf{y}}_k \triangleq \mathbf{y}_{k,t-1}$; $\bar{k} \triangleq k_{t-1}$; $\underline{\mathbf{y}}_k \triangleq \underline{\mathbf{y}}_{k,t}$; $\bar{\mathbf{y}}_m \triangleq \bar{\mathbf{y}}_{m,t}$; $f_A \triangleq f(\mathbf{s}_t | \mathbf{s}_{t-1})$; $f_k \triangleq f(\underline{\mathbf{y}}_{k,t} | \mathbf{y}_{k,t-1})$; $\mathbf{g} \triangleq f(\mathbf{g}_t | \mathbf{s}_t)$; $a_k \triangleq a_{k,t}$; $b_m \triangleq b_{m,t}$; $q_k \triangleq q(\underline{\mathbf{y}}_{k,t}, a_{k,t}, \mathbf{s}_t; \mathbf{z}_t)$; $h_m \triangleq h(\bar{\mathbf{y}}_{m,t}, b_{m,t}, \mathbf{s}_t; \mathbf{z}_{m,t})$; $\psi_{k,m} \triangleq \psi(a_{k,t}, b_{m,t})$.

into (12), and (3), (12), and (17) into (11)—is

$$f(\mathbf{y}_{0:t}, \mathbf{s}_{0:t}, \mathbf{a}_{1:t}, \mathbf{b}_{1:t} | \mathbf{g}_{1:t}, \mathbf{z}_{1:t})$$

$$\propto f(\mathbf{s}_0) f(\mathbf{y}_0) \prod_{t'=1}^{t} f(\mathbf{s}_{t'} | \mathbf{s}_{t'-1}) f(\mathbf{g}_{t'} | \mathbf{s}_{t'})$$

$$\times \left[\prod_{k=1}^{k_{t'-1}} f(\underline{\mathbf{y}}_{k,t'} | \mathbf{y}_{k,t'-1}) q(\underline{\mathbf{y}}_{k,t'}, a_{k,t'}, \mathbf{s}_{t'}; \mathbf{z}_{t'}) \right.$$

$$\left. \times \prod_{m=1}^{m_{t'}} \psi(a_{k,t'}, b_{m,t'}) \right] \prod_{m'=1}^{m_{t'}} h(\bar{\mathbf{y}}_{m',t'}, b_{m',t'}, \mathbf{s}_{t'}; \mathbf{z}_{m',t'}),$$

$$(21)$$

where $q(\cdot) \triangleq q_1(\cdot) q_2(\cdot)$ and $h(\cdot) \triangleq h_1(\cdot) h_2(\cdot)$. Direct marginalization of this joint posterior pdf for the computation of the marginal posterior pdfs/pmfs mentioned in Section III-A is generally unfeasible in reasonable time, as it requires high-dimensional integration and summation. Approximations at time t of these marginal pdfs/pmfs—called *beliefs* and referred to as $\tilde{f}_t(\cdot)$—can be efficiently obtained by applying the SPA on a factor graph [19], [20], carefully devised from the factorization in (21).

Such factor graph, illustrated for a single time step in Fig. 3, contains loops: an inner loop involving the data association variables $a_{k,t}$ and $b_{m,t}$, and an outer loop involving the AUV state $\mathbf{s}_t$ and factor nodes $q(\cdot)$ and $h(\cdot)$. Therefore, a scheduling of the messages is defined based on the following rules: (i) messages are not sent backward in time; (ii) iterative message passing is only performed for the data association, i.e., for the inner loop. More specifically, at each time t, the *inbound* messages—from outside to inside the blue dashed rectangle—are

computed first. These messages represent the prediction of the legacy PO states and AUV states, and are computed assuming that all the *outbound* messages—from inside to outside the blue dashed rectangle—are equal to one. The inbound messages are then employed within the inner loop for data association. When all the iterations of the inner loop are performed, the outbound messages are calculated and eventually used to compute the beliefs of the PO states. Next, we provide expressions of the messages combining the scheduling rules stated above and the generic SPA rules provided in [19]. The messages are all denoted by $\zeta_{\alpha \to \beta}(\cdot)$, where α and β are, respectively, the origin and destination nodes of the message. Moreover, we assume that the beliefs are normalized, i.e., $\int \tilde{f}_t(\alpha) d\alpha = 1$.

B. Inbound Messages

The inbound messages from variable node "$\mathbf{s}$" to factor node "q_k", i.e., $\zeta_{\mathbf{s} \to q_k}(\mathbf{s}_t)$, and from variable node "$\mathbf{s}$" to factor node "h_m", i.e., $\zeta_{\mathbf{s} \to h_m}(\mathbf{s}_t)$, represent the prediction of the AUV state and its refinement with navigation data. Recalling that the inbound messages are computed assuming that the outbound messages are all equal to one, the expressions of the messages $\zeta_{\mathbf{s} \to q_k}(\mathbf{s}_t)$ and $\zeta_{\mathbf{s} \to h_m}(\mathbf{s}_t)$ coincide; for them, we use the common notation $\zeta_{\mathbf{s}}(\mathbf{s}_t)$, that is,

$$\zeta_{\mathbf{s}}(\mathbf{s}_t) \triangleq \zeta_{\mathbf{s} \to q_k}(\mathbf{s}_t) = \zeta_{\mathbf{s} \to h_m}(\mathbf{s}_t)$$

$$= f(\mathbf{g}_t | \mathbf{s}_t) \int \tilde{f}_{t-1}(\mathbf{s}_{t-1}) f(\mathbf{s}_t | \mathbf{s}_{t-1}) d\mathbf{s}_{t-1}, \quad (22)$$

where $\tilde{f}_{t-1}(\cdot)$ is the belief computed at previous time $t-1$, whose expression is later provided in Section IV-E. For convenience, we also introduce the following constant:

$$\zeta_{\mathbf{s}}^0 = \int \zeta_{\mathbf{s}}(\mathbf{s}_t) d\mathbf{s}_t. \quad (23)$$

The inbound message from variable node "$\underline{\mathbf{y}}_k$" to factor node "q_k", representing the prediction of the legacy PO k, is computed as follows:

$$\zeta_{\underline{\mathbf{y}}_k \to q_k}(\underline{\mathbf{y}}_{k,t}) = \zeta_{\underline{\mathbf{y}}_k \to q_k}(\underline{\mathbf{x}}_{k,t}, \underline{\tau}_{k,t}, \underline{r}_{k,t})$$

$$= \sum_{r_{k,t-1}=0}^{1} \sum_{\tau_{k,t-1}=1}^{C} \int \tilde{f}_{t-1}(\mathbf{x}_{k,t-1}, \tau_{k,t-1}, r_{k,t-1})$$

$$\times f(\underline{\mathbf{x}}_{k,t}, \underline{\tau}_{k,t}, \underline{r}_{k,t} | \mathbf{x}_{k,t-1}, \tau_{k,t-1}, r_{k,t-1}) d\mathbf{x}_{k,t-1}.$$

Note that, since the belief $\tilde{f}_{t-1}(\cdot)$ is normalized, the message $\zeta_{\underline{\mathbf{y}}_k \to q_k}(\underline{\mathbf{x}}_{k,t}, \underline{\tau}_{k,t}, \underline{r}_{k,t})$ is also normalized, i.e.,

$$\sum_{r_{k,t}=0}^{1} \sum_{\underline{\tau}_{k,t}=1}^{C} \int \zeta_{\underline{\mathbf{y}}_k \to q_k}(\underline{\mathbf{x}}_{k,t}, \underline{\tau}_{k,t}, \underline{r}_{k,t}) d\underline{\mathbf{x}}_{k,t} = 1. \quad (24)$$

Furthermore, according to the definitions (4)–(5), and recalling that the POs are stationary and that their class does not change over time, the message

$\zeta_{\underline{\mathbf{y}}_k \to q_k}(\underline{\mathbf{x}}_{k,t}, \underline{\tau}_{k,t}, \underline{r}_{k,t})$ for $\underline{r}_{k,t} = 1$ becomes

$$\zeta_{\underline{\mathbf{y}}_k \to q_k}(\underline{\mathbf{x}}_{k,t}, \underline{\tau}_{k,t}, \underline{r}_{k,t} = 1) = \tilde{f}_{t-1}(\underline{\mathbf{x}}_{k,t}, \underline{\tau}_{k,t}, \underline{r}_{k,t} = 1). \quad (25)$$

Finally, the inbound message from variable node "$\overline{\mathbf{y}}_m$" to factor node "h_m" is equal to one, i.e.,

$$\zeta_{\overline{\mathbf{y}}_m \to h_m}(\overline{\mathbf{y}}_{m,t}) = \zeta_{\overline{\mathbf{y}}_m \to h_m}(\overline{\mathbf{x}}_{m,t}, \overline{\tau}_{m,t}, \overline{r}_{m,t}) = 1, \quad (26)$$

since "$\overline{\mathbf{y}}_m$" is a leaf variable node of the factor graph.

C. SPA-Based Data Association

The SPA-based data association is an iterative procedure that allows to compute accurate approximations of the marginal posterior data association pmfs, i.e., $p(a_{k,t}|\mathbf{g}_{1:t}, \mathbf{z}_{1:t})$ and $p(b_{m,t}|\mathbf{g}_{1:t}, \mathbf{z}_{1:t})$ [30]. Practically, the SPA-based data association step converts the messages $\zeta_{q_k \to a_k}(a_{k,t})$ and $\zeta_{h_m \to b_m}(b_{m,t})$, into the messages $\zeta_{a_k \to q_k}(a_{k,t})$ and $\zeta_{b_m \to h_m}(b_{m,t})$. Expressions of the latter messages are provided in [26, Sec. IX-A3], whereas details of the messages $\zeta_{q_k \to a_k}(a_{k,t})$ and $\zeta_{h_m \to b_m}(b_{m,t})$ are given below.

The message from factor node "q_k" to variable node "a_k" is computed as

$$\zeta_{q_k \to a_k}(a_{k,t}) = \sum_{\underline{r}_{k,t}=0}^{1} \sum_{\underline{\tau}_{k,t}=1}^{C} \iint \zeta_{\underline{\mathbf{y}}_k \to q_k}(\underline{\mathbf{x}}_{k,t}, \underline{\tau}_{k,t}, \underline{r}_{k,t})$$
$$\times \zeta_{\mathbf{s}}(\mathbf{s}_t) q(\underline{\mathbf{x}}_{k,t}, \underline{\tau}_{k,t}, \underline{r}_{k,t}, a_{k,t}, \mathbf{s}_t; \mathbf{z}_t) d\underline{\mathbf{x}}_{k,t} d\mathbf{s}_t.$$

Using definitions (13)–(14) and (18)–(19), constant (23), condition (24), and message (25), we obtain for $a_{k,t} = 0$

$$\zeta_{q_k \to a_k}(a_{k,t} = 0)$$
$$= \zeta_{\mathbf{s}}^0 - \iint \zeta_{\mathbf{s}}(\mathbf{s}_t) \left[\sum_{\underline{\tau}_{k,t}=1}^{C} P_{\mathrm{d}}(\underline{\mathbf{x}}_{k,t}, \underline{\tau}_{k,t}, \mathbf{s}_t) \right.$$
$$\left. \times \tilde{f}_{t-1}(\underline{\mathbf{x}}_{k,t}, \underline{\tau}_{k,t}, 1) \right] d\underline{\mathbf{x}}_{k,t} d\mathbf{s}_t,$$

and for $a_{k,t} \in \{1, \dots, m_t\}$

$$\zeta_{q_k \to a_k}(a_{k,t} = m)$$
$$= \frac{1}{\mu_0 f_{\mathrm{FA}}(\mathbf{z}_{m,t})} \iint \zeta_{\mathbf{s}}(\mathbf{s}_t) \left[\sum_{\underline{\tau}_{k,t}=1}^{C} P_{\mathrm{d}}(\underline{\mathbf{x}}_{k,t}, \underline{\tau}_{k,t}, \mathbf{s}_t) \right.$$
$$\left. \times \tilde{f}_{t-1}(\underline{\mathbf{x}}_{k,t}, \underline{\tau}_{k,t}, 1) f(\mathbf{z}_{m,t}|\underline{\mathbf{x}}_{k,t}, \underline{\tau}_{k,t}, \mathbf{s}_t) \right] d\underline{\mathbf{x}}_{k,t} d\mathbf{s}_t.$$

Similarly, the message from factor node "h_m" to variable node "b_m" is computed as

$$\zeta_{h_m \to b_m}(b_{m,t})$$
$$= \sum_{\overline{r}_{m,t}=0}^{1} \sum_{\overline{\tau}_{m,t}=1}^{C} \iint \zeta_{\overline{\mathbf{y}}_m \to h_m}(\overline{\mathbf{x}}_{m,t}, \overline{\tau}_{m,t}, \overline{r}_{m,t})$$
$$\times \zeta_{\mathbf{s}}(\mathbf{s}_t) h(\overline{\mathbf{x}}_{m,t}, \overline{\tau}_{m,t}, \overline{r}_{m,t}, b_{m,t}, \mathbf{s}_t; \mathbf{z}_{m,t}) d\overline{\mathbf{x}}_{m,t} d\mathbf{s}_t.$$

Using definitions (15)–(16) and (20), constant (23), and message (26), we obtain for $b_{m,t} = 0$

$$\zeta_{h_m \to b_m}(b_{m,t} = 0)$$
$$= \zeta_{\mathbf{s}}^0 + \frac{\mu_{\mathrm{N}}}{\mu_0 f_{\mathrm{FA}}(\mathbf{z}_{m,t})} \iint \zeta_{\mathbf{s}}(\mathbf{s}_t) \left[\sum_{\overline{\tau}_{m,t}=1}^{C} f_{\mathrm{N}}(\overline{\mathbf{x}}_{m,t}, \overline{\tau}_{m,t}) \right.$$
$$\left. \times f(\mathbf{z}_{m,t}|\overline{\mathbf{x}}_{m,t}, \overline{\tau}_{m,t}, \mathbf{s}_t) \right] d\overline{\mathbf{x}}_{m,t} d\mathbf{s}_t,$$

and $\zeta_{h_m \to b_m}(b_{m,t}) = \zeta_{\mathbf{s}}^0$ for $b_{m,t} \in \{1, \dots, k_{t-1}\}$.

D. Outbound Messages

Once the iterations of the inner loop for data association are performed, and the messages $\zeta_{a_k \to q_k}(a_{k,t})$ and $\zeta_{b_m \to h_m}(b_{m,t})$ are available, the outbound messages are computed and eventually used to obtain the updated beliefs. The outbound message from factor node "q_k" to variable node "$\mathbf{s}$", representing the contribution of the legacy PO k to the inference of the AUV state $\mathbf{s}_t$, is computed as follows:

$$\zeta_{q_k \to \mathbf{s}}(\mathbf{s}_t) = \sum_{\underline{r}_{k,t}=0}^{1} \sum_{\underline{\tau}_{k,t}=1}^{C} \sum_{a_{k,t}=0}^{m_t} \int \zeta_{\underline{\mathbf{y}}_k \to q_k}(\underline{\mathbf{x}}_{k,t}, \underline{\tau}_{k,t}, \underline{r}_{k,t})$$
$$\times \zeta_{a_k \to q_k}(a_{k,t}) q(\underline{\mathbf{x}}_{k,t}, \underline{\tau}_{k,t}, \underline{r}_{k,t}, a_{k,t}, \mathbf{s}_t; \mathbf{z}_t) d\underline{\mathbf{x}}_{k,t}.$$

As before, using definitions (13)–(14) and (18)–(19), condition (24), and message (25), the message $\zeta_{q_k \to \mathbf{s}}(\mathbf{s}_t)$ can be rewritten as

$$\zeta_{q_k \to \mathbf{s}}(\mathbf{s}_t) = \zeta_{a_k \to q_k}(a_{k,t} = 0) - \sum_{\underline{\tau}_{k,t}=1}^{C} \int P_{\mathrm{d}}(\underline{\mathbf{x}}_{k,t}, \underline{\tau}_{k,t}, \mathbf{s}_t)$$
$$\times \tilde{f}_{t-1}(\underline{\mathbf{x}}_{k,t}, \underline{\tau}_{k,t}, 1) \mathfrak{f}(\underline{\mathbf{x}}_{k,t}, \underline{\tau}_{k,t}, \mathbf{s}_t; \mathbf{z}_t) d\underline{\mathbf{x}}_{k,t},$$

where

$$\mathfrak{f}(\underline{\mathbf{x}}_{k,t}, \underline{\tau}_{k,t}, \mathbf{s}_t; \mathbf{z}_t) \triangleq \zeta_{a_k \to q_k}(a_{k,t} = 0)$$
$$- \frac{1}{\mu_0} \sum_{m=1}^{m_t} \zeta_{a_k \to q_k}(a_{k,t} = m) \frac{f(\mathbf{z}_{m,t}|\underline{\mathbf{x}}_{k,t}, \underline{\tau}_{k,t}, \mathbf{s}_t)}{f_{\mathrm{FA}}(\mathbf{z}_{m,t})}.$$

Similarly, the outbound message from factor node "h_m" to variable node "$\mathbf{s}$", representing the contribution of the new PO m to the inference of the AUV state $\mathbf{s}_t$, is computed as follows:

$$\zeta_{h_m \to \mathbf{s}}(\mathbf{s}_t)$$
$$= \sum_{\overline{r}_{m,t}=0}^{1} \sum_{\overline{\tau}_{m,t}=1}^{C} \sum_{b_{m,t}=0}^{k_{t-1}} \int \zeta_{\overline{\mathbf{y}}_m \to h_m}(\overline{\mathbf{x}}_{m,t}, \overline{\tau}_{m,t}, \overline{r}_{m,t})$$
$$\times \zeta_{b_m \to h_m}(b_{m,t}) h(\overline{\mathbf{x}}_{m,t}, \overline{\tau}_{m,t}, \overline{r}_{m,t}, b_{m,t}, \mathbf{s}_t; \mathbf{z}_{m,t}) d\overline{\mathbf{x}}_{m,t}.$$

Using definitions (15)–(16) and (20), and message (26), the message $\zeta_{h_m \to s}(s_t)$ can be rewritten as

$$\zeta_{h_m \to s}(s_t) = \sum_{k=1}^{k_{t-1}} \zeta_{b_m \to h_m}(b_{m,t} = k)$$

$$+ \zeta_{b_m \to h_m}(b_{m,t} = 0)\left[1 + \frac{\mu_N}{\mu_0 f_{FA}(z_{m,t})}\right.$$

$$\left. \times \sum_{\bar\tau_{m,t}=1}^{C} \int f_N(\bar{x}_{m,t}, \bar\tau_{m,t}) f(z_{m,t}|\bar{x}_{m,t}, \bar\tau_{m,t}, s_t)\, \mathrm{d}\bar{x}_{m,t}\right].$$

Finally, the outbound messages from factor node "q_k" to variable node "$\underline{y}_k$", and from factor node "h_m" to variable node "$\bar{y}_m$", are computed as, respectively,

$$\zeta_{q_k \to \underline{y}_k}(\underline{y}_{k,t}) = \int \zeta_s(s_t) \prod_{\substack{k'=1 \\ k' \neq k}}^{k_{t-1}} \zeta_{q_{k'} \to s}(s_t) \prod_{m=1}^{m_t} \zeta_{h_m \to s}(s_t)$$

$$\times \left[\sum_{a_{k,t}=0}^{m_t} \zeta_{a_k \to q_k}(a_{k,t}) q(\underline{y}_{k,t}, a_{k,t}, s_t; z_t)\right] \mathrm{d}s_t$$

and

$$\zeta_{h_m \to \bar{y}_m}(\bar{y}_{m,t}) = \int \zeta_s(s_t) \prod_{k=1}^{k_{t-1}} \zeta_{q_k \to s}(s_t) \prod_{\substack{m'=1 \\ m' \neq m}}^{m_t} \zeta_{h_{m'} \to s}(s_t)$$

$$\times \left[\sum_{b_{m,t}=0}^{k_{t-1}} \zeta_{b_m \to h_m}(b_{m,t}) h(\bar{y}_{m,t}, b_{m,t}, s_t; z_{m,t})\right] \mathrm{d}s_t.$$

E. Beliefs Computation

The final step of the proposed algorithm regards the computation of the beliefs at current time t of the legacy PO states, i.e., $\tilde{f}_t(\underline{y}_{k,t}), k \in \{1, \ldots, k_{t-1}\}$, and the new PO states, i.e., $\tilde{f}_t(\bar{y}_{m,t}), m \in \{1, \ldots, m_t\}$. The belief $\tilde{f}_t(\underline{y}_{k,t})$ is computed—up to a constant factor—as the product of the messages that are passed (in opposite directions) over the edge connecting variable node "$\underline{y}_k$" and factor node "q_k" [19], that is,

$$\tilde{f}_t(\underline{y}_{k,t}) \propto \zeta_{q_k \to \underline{y}_k}(\underline{y}_{k,t})\, \zeta_{\underline{y}_k \to q_k}(\underline{y}_{k,t}).$$

The constant factor (not reported) ensures that the belief normalizes to 1. Similarly, the belief $\tilde{f}_t(\bar{y}_{m,t})$ is computed as the product of the messages that are passed (in opposite directions) over the edge connecting variable node "$\bar{y}_m$" and factor node "h_m", that is,

$$\tilde{f}_t(\bar{y}_{m,t}) \propto \zeta_{h_m \to \bar{y}_m}(\bar{y}_{m,t})\, \zeta_{\bar{y}_m \to h_m}(\bar{y}_{m,t})$$

$$= \zeta_{h_m \to \bar{y}_m}(\bar{y}_{m,t}).$$

Eventually, the belief of the AUV state $\tilde{f}_t(s_t)$ is also computed as it is needed for the computation of the message (22) at the next step $t+1$; this belief is calculated as

the product of all the messages directed toward variable node "s" [19], that is,

$$\tilde{f}_t(s_t) \propto \zeta_s(s_t) \prod_{k=1}^{k_{t-1}} \zeta_{q_k \to s}(s_t) \prod_{m=1}^{m_t} \zeta_{h_m \to s}(s_t).$$

F. Implementation Details

The proposed SPA-based algorithm for autonomous mapping of underwater objects is implemented following a particle-based approach [31] that scales quadratically with the number of particles and the number of legacy POs, and scales linearly with the number of measurements and the number of iterations of the data association loop. As mentioned in Section II-B, in order to keep a tractable number of POs over time, a pruning step is performed. Specifically, any PO $k \in \{1, \ldots, k_t\}$ whose posterior probability of existence, i.e., $p(r_{k,t} = 1| g_{1:t}, z_{1:t})$, is below a given threshold P_{th}, is removed and is not carried over to the next time step $t+1$. Moreover, to avoid PO particle impoverishment, especially due to the stationarity of the considered objects, a simple roughening strategy is employed [32].

V. SIMULATION RESULTS

A. Scenario Description

Performance of the proposed SPA-based algorithm for autonomous mapping of underwater objects is evaluated in a typical MCM mission. An AUV is programmed to survey an area of 0.25 km^2 with 5 MLOs and 45 non-MLOs by following a lawnmower pattern. The scenario is illustrated in Fig. 4, with the AUV trajectory shown as an orange solid line, and MLOs and non-MLOs as, respectively, red diamonds and green dots. The AUV state includes position and velocity in Cartesian coordinate, as well as the turn rate v_t, i.e., $s_t = \left[s_{t,p}^T, s_{t,v}^T, v_t\right]^T$. The AUV kinematic model employed in the proposed algorithm and used to evaluate the pdf $f(s_t|s_{t-1})$ is the nearly constant turn model, that is (cf. eq. (1)),

$$s_t = \varepsilon(s_{t-1}, u_t) = F(s_{t-1}) + G(s_{t-1})u_t, \qquad (27)$$

where $F(\cdot)$ and $G(\cdot)$ are defined in [33, eqs. (6) and (7a)], and u_t is a 2D zero-mean Gaussian process noise whose covariance is diag$(\sigma_{lin}^2, \sigma_{ang}^2)$.

The AUV moves at 1.5 m/s, produces an SAS image every $T = 33$ s, and completes the survey in approximately 2.8 h, i.e., in 305 time steps. The dimensions of the SAS tile along and across the direction of travel are, respectively, $\Delta\eta_1 = 50$ m and $\Delta\eta_2 = 110$ m, and its position with respect to the AUV is defined by $\eta_1^{(1)} = 0$ and $\eta_2^{(1)} = 20$ m (see Fig. 2). The ATR algorithm detects objects within SAS tiles with probability $p_d(\tau_{k,t}) = p_d = 0.9$, and distinguishes among $C = 2$ classes, i.e., MLOs ($c = 1$) and non-MLOs ($c = 2$); the vector parameters α_1 and α_2 used for simulating the probabilities
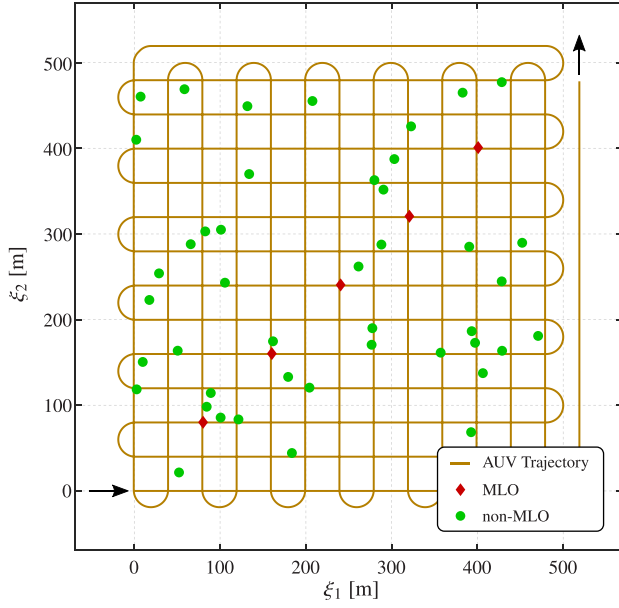
Figure 4. Illustration of the simulated scenario. The orange solid line represents the trajectory of the AUV, with the arrows indicating the beginning and the end of the trajectory. MLOs and non-MLOs are depicted as, respectively, red diamonds and green dots.
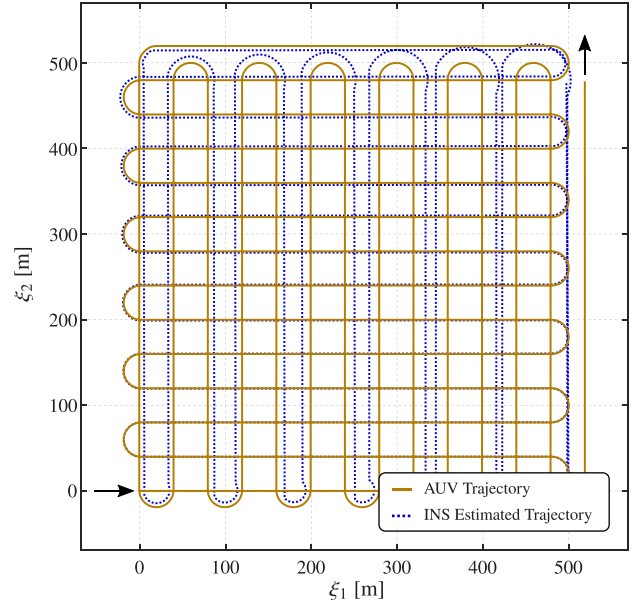

Figure 5. Illustration of the simulated scenario. The orange solid line represents the trajectory of the AUV, and the blue dotted line represents the trajectory estimated by the INS following the model in (28)–(30) with $\lambda_0 = \pi/4$ and $\epsilon_p = 7.5$ m/h^2. The arrows indicate the beginning and the end of the trajectory.

$\pi_{m,t}^{(1)}$ as well as for the evaluation of the pdf $f(\pi_{m,t}^{(1)}|\tau_{k,t})$ in (7) are set to $\boldsymbol{\alpha}_1 = [6, 2]^\mathrm{T}$ and $\boldsymbol{\alpha}_2 = [2, 6]^\mathrm{T}$, respectively. The object-generated measurements are simulated according to the following model, that is,

$$
\begin{aligned}
\boldsymbol{\ell}_{m,t} &= \boldsymbol{\gamma}_\mathrm{O}\big(\boldsymbol{\theta}(\boldsymbol{x}_{k,t}; \boldsymbol{s}_t), \boldsymbol{\omega}_{m,t}\big) \\
&= \boldsymbol{R}(\angle \boldsymbol{s}_{t,\mathrm{v}})\big[\boldsymbol{x}_{k,t} - \boldsymbol{s}_{t,\mathrm{p}}\big] + \boldsymbol{\omega}_{m,t},
\end{aligned}
$$

where $\boldsymbol{\omega}_{m,t}$ is a 2D zero-mean Gaussian process noise with covariance $\sigma_\omega^2 \mathbf{I}$ with $\sigma_\omega = 1$ m. The same model is used to evaluate the likelihood $f(\boldsymbol{\ell}_{m,t}|\boldsymbol{x}_{k,t}, \boldsymbol{s}_t)$. The mean number of clutter-generated measurements within both the port side and starboard side tiles is $\mu_0 = 0.1$.

The AUV's INS provides navigation data $\boldsymbol{g}_t \in \mathbb{R}^3$ — that includes 2D position and heading—generated according to the following model:

$$
\boldsymbol{g}_t = \big[\boldsymbol{s}_{t,\mathrm{p}}^\mathrm{T}, \angle \boldsymbol{s}_{t,\mathrm{v}}\big]^\mathrm{T} + \boldsymbol{d}_t, \tag{28}
$$

where $\boldsymbol{d}_t$ is a 3D component that emulates the INS drift. For this analysis, the INS error model described in [34] is employed. Specifically, the position error has mean and variance that accumulate, respectively, quadratically and cubically over time [34, Table III]; for the heading error, instead, both mean and variance accumulate linearly over time [34, Table II]. Therefore, $\boldsymbol{d}_t$ is modeled as a 3D Gaussian process with time-varying mean

$$
\frac{1}{2}\begin{bmatrix} \epsilon_\mathrm{p}\cos(\angle \boldsymbol{s}_{t,\mathrm{v}} + \lambda_0)(tT)^2 \\ \epsilon_\mathrm{p}\sin(\angle \boldsymbol{s}_{t,\mathrm{v}} + \lambda_0)(tT)^2 \\ (-1)^\iota 2\epsilon_\mathrm{h}(tT) \end{bmatrix}, \tag{29}
$$

and time-varying covariance

$$
\begin{aligned}
\frac{1}{3}\mathrm{diag}\Big(&\varsigma_\mathrm{p}^2 (tT)^3 \cos^2(\angle \boldsymbol{s}_{t,\mathrm{v}} + \lambda_0), \dots \\
&\varsigma_\mathrm{p}^2 (tT)^3 \sin^2(\angle \boldsymbol{s}_{t,\mathrm{v}} + \lambda_0), \dots \\
&3\varsigma_\mathrm{h}^2 (tT)\Big),
\end{aligned} \tag{30}
$$

where $\lambda_0 \in (0, 2\pi)$ and $\iota \in \{0, 1\}$. Parameters ϵ_p and ϵ_h drive, respectively, the quadratic growth of the position drift, and the linear growth of the heading drift, whereas ς_p^2 and ς_h^2 control, respectively, the cubic growth of the position error variance—for each Cartesian coordinate—and the linear growth of the heading error variance. Note that the INS drift is related to the AUV local reference system, which explains the use of $\angle \boldsymbol{s}_{t,\mathrm{v}}$ in (29)–(30); finally, ι is used to select a positive or negative heading drift, and λ_0 is used to balance the position drift over the two Cartesian coordinates. As an example, with $\lambda_0 = 0$ the AUV's position estimated by the INS is *advanced* with respect to the true AUV's position; with $\lambda_0 = \pi$, instead, the AUV's position estimated by the INS is *delayed* with respect to the true AUV's position. Figure 5 shows an example with $\lambda_0 = \pi/4$ and $\epsilon_\mathrm{p} = 7.5$ m/h^2: as time goes by, the INS provides AUV position estimates that are quadratically farther from the actual trajectory.

The INS error model defined by (29)–(30) is assumed partly unknown when running the proposed algorithm. Specifically, we consider unknown the mean (29) as well as the angle λ_0, wheres we assume known the cubic growth law of the position error variance and the linear growth law of the heading error variance. There-

fore, the navigation data model used to evaluate the likelihood $f(\boldsymbol{g}_t|\boldsymbol{s}_t)$ is set to (cf. eq. (2)),

$$\boldsymbol{g}_t = \boldsymbol{\gamma}_{\mathrm{A}}(\boldsymbol{s}_t, \boldsymbol{v}_t) = \left[\boldsymbol{s}_{t,\mathrm{p}}^{\mathrm{T}}, \angle \boldsymbol{s}_{t,\mathrm{v}}\right]^{\mathrm{T}} + \boldsymbol{v}_t,$$

where $\boldsymbol{v}_t$ is a 3D zero-mean Gaussian process noise with time-varying covariance $\mathrm{diag}(\sigma_{\mathrm{p},t}^2, \sigma_{\mathrm{p},t}^2, \sigma_{\mathrm{h},t}^2)$, where

$$\sigma_{\mathrm{p},t}^2 = \frac{1}{3}\sigma_{\mathrm{p}}^2(tT)^3 \quad \text{and} \quad \sigma_{\mathrm{h},t}^2 = \sigma_{\mathrm{h}}^2(tT)$$

with $\sigma_{\mathrm{p}} = 3\,\varsigma_{\mathrm{p}}$ and $\sigma_{\mathrm{h}} = 3\,\varsigma_{\mathrm{h}}$.

Remark The INS usually provides its output much faster than $T = 33$ s. For this analysis, we assume that navigation data are available every second; this means that between any two time steps $t-1$ and t, the INS provides 32 navigation outputs. Therefore, between any two time steps, prediction and update of the AUV state are performed every second by only using the INS output; this is equivalent to run the SPA-based algorithm on a factor graph only composed by the variable nodes "$\boldsymbol{s}^-$" and "$\boldsymbol{s}$", and the factor nodes "f_{A}" and "$\boldsymbol{g}$" (see Fig. 3). Then, when both the SAS image and navigation data are available at time t, the full SPA-based algorithm described in Section IV is run. Finally, since the AUV state prediction is performed every second, the parameters σ_{lin} and σ_{ang} defining the process noise $\boldsymbol{u}_t$ in (27) and used to evaluate the pdf $f(\boldsymbol{s}_t|\boldsymbol{s}_{t-1})$ are set to $\sigma_{\mathrm{lin}} = 0.5$ m/s^2 and $\sigma_{\mathrm{ang}} = 20$ deg/s^2.

B. Results

The results obtained with the *proposed* SPA-based algorithm for autonomous mapping of underwater objects are compared with three alternative SPA-based algorithms; these alternative algorithms all assume that the AUV state at time t is known. The first one is *clairvoyant* in that it knows the "true" AUV state at time t; this is clearly used as a benchmark, since this information is not available in practice. The second alternative algorithm, referred to as *INS-plain*, considers the navigation data $\boldsymbol{g}_t$ as AUV state at current time t, with no further processing. The third alternative algorithm exploits the navigation data provided by the INS every second to sequentially infer the AUV state at time t by means of a particle filter, thus called *INS-filter*. This differs from the proposed algorithm in that it does not exploit the information readily available on the detected objects to refine the AUV state estimate, and, on the other hand, it uses only the estimated AUV position—and not its belief—to make inference about the existence and location of the objects. The results shown hereafter are averaged over 100 Monte Carlo runs; each run differs for the positions of the non-MLOs that are uniformly located in the area of interest, and for the values of $\lambda_0 \in (0, 2\pi)$ and $\iota \in \{0, 1\}$ used in (29)–(30) for the generation of the INS drifts. Moreover, 1000 particles are used to describe the SPA beliefs and messages, and the prior distributions $f_{\mathrm{n}}(\overline{\boldsymbol{x}}_{m,t})$ and $f_{\mathrm{n}}(\overline{\tau}_{m,t})$ related to the position and class of a new PO are, respectively, uniform over the SAS tile, and
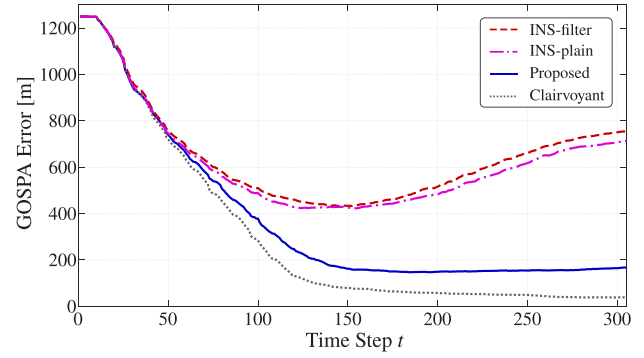

Figure 6. GOSPA errors obtained with the proposed algorithm and with three alternative algorithms, namely, clairvoyant, INS-plain, and INS-filter.

equal to $f_{\mathrm{n}}(\overline{\tau}_{m,t}) = 0.5$ for $\overline{\tau}_{m,t} \in \{1, 2\}$. The remaining parameters are set to $\epsilon_{\mathrm{p}} = 7.5$ m/h^2, $\epsilon_{\mathrm{h}} = 1$ deg/h, $\varsigma_{\mathrm{p}} = 7.5$ m/h$^{\frac{3}{2}}$, $\varsigma_{\mathrm{h}} = 0.6$ deg/h$^{\frac{1}{2}}$, $\mu_{\mathrm{N}} = 10^{-3}$, $P_{\mathrm{th}} = 10^{-4}$, and, unless otherwise stated, $E_{\mathrm{th}} = 0.8$.

The performance of the different algorithms is compared in Fig. 6 in terms of the Euclidean distance-based generalized optimal sub-pattern assignment (GOSPA) error [35], with cut-off parameter 50 m and order 1. The GOSPA metric accounts for localization errors for correctly confirmed objects, errors for missed objects, and false objects (i.e., confirmed POs not corresponding to any actual object). As expected, the clairvoyant algorithm presents the lowest GOSPA error, since it assumes a perfect knowledge of the AUV state at each time t; the error is decreasing because more objects are observed and detected as the AUV surveys the area of interest. The proposed algorithm, the INS-plain, and the INS-filter approaches have GOSPA errors very similar to those obtained with the clairvoyant algorithm at the beginning of the mission; indeed, up to time step 50, the impact of the drift is limited. As the mission proceeds, we observe that the proposed algorithm clearly outperforms the INS-plain and INS-filter approaches, demonstrating the benefit of including the inference of the AUV state within the objects detection/estimation procedure. These results are confirmed by those reported in Fig. 7, which shows the number of correctly detected objects—those for which the distance between the estimated and true position is lower than 20 m—versus the number of false objects at the end of the mission. These curves are obtained by varying the existence threshold[2] E_{th}, and demonstrate the capability of the proposed algorithm to account for the uncertain AUV state and correctly detect a higher number of objects compared to the INS-plain and INS-filter approaches. Finally, Fig. 8 shows the cardinality—i.e., the number of detected objects, including potential false objects—obtained with the proposed algorithm and the three alternative approaches

---

[2]For the generation of the curves in Fig. 7, 20 values of the existence threshold E_{th} are selected evenly distributed on a log scale between a minimum value of 0.02 and a maximum value of 0.99.
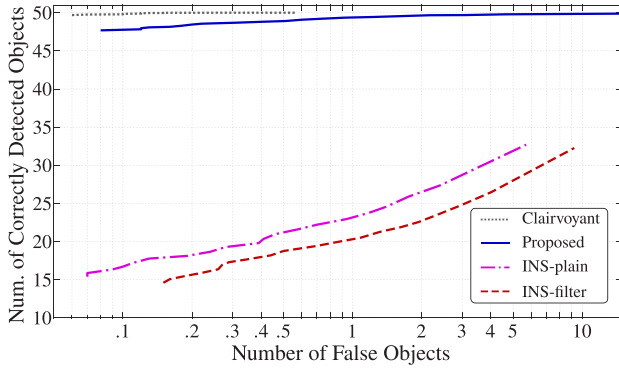
Figure 7. Number of correctly detected objects versus the number of false objects at the end of the mission obtained with the proposed algorithm and with three alternative algorithms, namely, clairvoyant, INS-plain, and INS-filter.

over time, and compares them with the true cardinality,[3] demonstrating the effectiveness of the proposed algorithm. The capability of the clairvoyant and proposed algorithms to correctly detect a higher number of objects clearly reflects into their ability to correctly classify them. Indeed, the clairvoyant and proposed algorithms reach an overall classification accuracy of 99%, compared to 47% and 45% obtained with, respectively, the INS-plain approach and the INS-filter approach. Lastly, as concerns the AUV position estimate, the proposed algorithm provides a time-averaged root-mean-square error (RMSE) of 10.9 m, while the INS-filter approach provides a time-averaged RMSE of 11.5 m. This moderate improvement of the proposed algorithm compared to the INS-filter approach is likely due to the fact that not all the objects are observable at all times; therefore, at each time t, the proposed algorithm only relies on a small set of detected objects to estimate the AUV position.

---

[3]The true cardinality is time-varying since more objects are observed as the AUV surveys the area of interest.
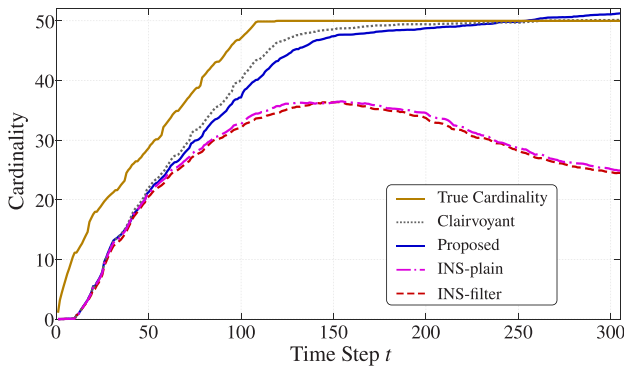

Figure 8. Cardinality over time obtained with the proposed algorithm and with three alternative algorithms, namely, clairvoyant, INS-plain, and INS-filter.

VI. CONCLUSIONS

Mapping of underwater objects is usually conducted with AUVs. A classic example is MCM operations, in which AUVs allow to operate from a distance in safe conditions. Independently of the type of application, the quality and value of the data acquired by an AUV are significantly influenced by the accuracy of its position. Because of the unavailability of GPS technologies below the sea surface, an AUV generally relies on an INS that calculates the position and heading of the vehicle by integrating values measured by accelerometers and gyroscopes available on-board. However, because of this integration, the inherent errors of these devices accumulate over time, resulting in position and orientation errors that increase over time.

This paper has proposed and described a Bayesian graph-based mapping algorithm that accounts for the inherent uncertainty of the AUV position. Exploiting the SPA, the proposed technique obtains a principled and intuitive approximation of the Bayesian inference needed for underwater object detection and estimation. The effectiveness of the proposed algorithm has been demonstrated in a simulated MCM scenario, which has shown the benefit of including the inference of the AUV position within the object detection/estimation procedure.

APPENDIX

Here, we derive the factorization in (11) of the joint posterior pdf $f(\boldsymbol{y}_{0:t}, \boldsymbol{s}_{0:t}, \boldsymbol{a}_{1:t}, \boldsymbol{b}_{1:t} | \boldsymbol{g}_{1:t}, \boldsymbol{z}_{1:t})$. Since the measurements $\boldsymbol{z}_{1:t}$ are observed, hence known, the joint vector of numbers of measurements $\boldsymbol{m}_{1:t}$ is also known, that is, $f(\boldsymbol{y}_{0:t}, \boldsymbol{s}_{0:t}, \boldsymbol{a}_{1:t}, \boldsymbol{b}_{1:t} | \boldsymbol{g}_{1:t}, \boldsymbol{z}_{1:t}) = f(\boldsymbol{y}_{0:t}, \boldsymbol{s}_{0:t}, \boldsymbol{a}_{1:t}, \boldsymbol{b}_{1:t} | \boldsymbol{g}_{1:t}, \boldsymbol{z}_{1:t}, \boldsymbol{m}_{1:t})$. Then, assuming that all the variables—joint PO state, AUV state, data association variables, navigation data, and measurements—at time t are conditionally independent of the past variables given the joint PO state and AUV state at previous time $t-1$, we obtain the factorization in (32). Recalling from Section II-B that $\boldsymbol{y}_t$ is the vector stacking the k_{t-1} legacy PO states and the m_t new PO states at time t, that is, $\boldsymbol{y}_t = [\underline{\boldsymbol{y}}_t^{\mathrm{T}}, \bar{\boldsymbol{y}}_t^{\mathrm{T}}]^{\mathrm{T}}$, each factor $f(\boldsymbol{y}_t, \boldsymbol{s}_t, \boldsymbol{a}_t, \boldsymbol{b}_t, \boldsymbol{g}_t, \boldsymbol{z}_t, m_t | \boldsymbol{y}_{t-1}, \boldsymbol{s}_{t-1})$ of the product in (32) can be further expressed as

$$f(\boldsymbol{y}_t, \boldsymbol{s}_t, \boldsymbol{a}_t, \boldsymbol{b}_t, \boldsymbol{g}_t, \boldsymbol{z}_t, m_t | \boldsymbol{y}_{t-1}, \boldsymbol{s}_{t-1})$$
$$= f(\bar{\boldsymbol{y}}_t, \boldsymbol{a}_t, \boldsymbol{b}_t, \boldsymbol{g}_t, \boldsymbol{z}_t, m_t | \underline{\boldsymbol{y}}_t, \boldsymbol{s}_t, \boldsymbol{y}_{t-1}, \boldsymbol{s}_{t-1})$$
$$\times f(\underline{\boldsymbol{y}}_t, \boldsymbol{s}_t | \boldsymbol{y}_{t-1}, \boldsymbol{s}_{t-1})$$
$$= f(\bar{\boldsymbol{y}}_t, \boldsymbol{a}_t, \boldsymbol{b}_t, \boldsymbol{g}_t, \boldsymbol{z}_t, m_t | \underline{\boldsymbol{y}}_t, \boldsymbol{s}_t) f(\underline{\boldsymbol{y}}_t | \boldsymbol{y}_{t-1}) f(\boldsymbol{s}_t | \boldsymbol{s}_{t-1})$$
$$= f(\bar{\boldsymbol{y}}_t, \boldsymbol{a}_t, \boldsymbol{b}_t, \boldsymbol{z}_t, m_t | \underline{\boldsymbol{y}}_t, \boldsymbol{s}_t) f(\boldsymbol{g}_t | \boldsymbol{s}_t)$$
$$\times f(\underline{\boldsymbol{y}}_t | \boldsymbol{y}_{t-1}) f(\boldsymbol{s}_t | \boldsymbol{s}_{t-1}), \tag{31}$$

where we assumed that PO states and AUV states evolve independently, and that navigation data and measurements are conditionally independent given the AUV

$$f\left(\boldsymbol{y}_{0:t}, \boldsymbol{s}_{0:t}, \boldsymbol{a}_{1:t}, \boldsymbol{b}_{1:t} \big| \boldsymbol{g}_{1:t}, \boldsymbol{z}_{1:t}, \boldsymbol{m}_{1:t}\right)$$

$$\propto f\left(\boldsymbol{y}_{0:t}, \boldsymbol{s}_{0:t}, \boldsymbol{a}_{1:t}, \boldsymbol{b}_{1:t}, \boldsymbol{g}_{1:t}, \boldsymbol{z}_{1:t}, \boldsymbol{m}_{1:t}\right)$$

$$= f\left(\boldsymbol{y}_t, \boldsymbol{s}_t, \boldsymbol{a}_t, \boldsymbol{b}_t, \boldsymbol{g}_t, \boldsymbol{z}_t, m_t \big| \boldsymbol{y}_{0:t-1}, \boldsymbol{s}_{0:t-1}, \boldsymbol{a}_{1:t-1}, \boldsymbol{b}_{1:t-1}, \boldsymbol{g}_{1:t-1}, \boldsymbol{z}_{1:t-1}, \boldsymbol{m}_{1:t-1}\right)$$

$$\times f\left(\boldsymbol{y}_{0:t-1}, \boldsymbol{s}_{0:t-1}, \boldsymbol{a}_{1:t-1}, \boldsymbol{b}_{1:t-1}, \boldsymbol{g}_{1:t-1}, \boldsymbol{z}_{1:t-1}, \boldsymbol{m}_{1:t-1}\right)$$

$$= f\left(\boldsymbol{y}_t, \boldsymbol{s}_t, \boldsymbol{a}_t, \boldsymbol{b}_t, \boldsymbol{g}_t, \boldsymbol{z}_t, m_t \big| \boldsymbol{y}_{t-1}, \boldsymbol{s}_{t-1}\right) \times f\left(\boldsymbol{y}_{0:t-1}, \boldsymbol{s}_{0:t-1}, \boldsymbol{a}_{1:t-1}, \boldsymbol{b}_{1:t-1}, \boldsymbol{g}_{1:t-1}, \boldsymbol{z}_{1:t-1}, \boldsymbol{m}_{1:t-1}\right)$$

$$= f(\boldsymbol{s}_0) f(\boldsymbol{y}_0) \prod_{t'=1}^{t} f\left(\boldsymbol{y}_{t'}, \boldsymbol{s}_{t'}, \boldsymbol{a}_{t'}, \boldsymbol{b}_{t'}, \boldsymbol{g}_{t'}, \boldsymbol{z}_{t'}, m_{t'} \big| \boldsymbol{y}_{t'-1}, \boldsymbol{s}_{t'-1}\right) \qquad (32)$$

state $\boldsymbol{s}_t$. Then, observing that the description of the data association given by $\boldsymbol{a}_t$ and $\boldsymbol{b}_t$ is redundant once m_t is observed—indeed, $\boldsymbol{a}_t$ can be derived from $\boldsymbol{b}_t$, and vice versa, when m_t is known [26] —, each factor $f(\bar{\boldsymbol{y}}_t, \boldsymbol{a}_t, \boldsymbol{b}_t, \boldsymbol{z}_t, m_t | \underline{\boldsymbol{y}}_t, \boldsymbol{s}_t)$ can be further expressed as

$$f(\bar{\boldsymbol{y}}_t, \boldsymbol{a}_t, \boldsymbol{b}_t, \boldsymbol{z}_t, m_t | \underline{\boldsymbol{y}}_t, \boldsymbol{s}_t)$$

$$= f(\boldsymbol{z}_t | \boldsymbol{y}_t, \boldsymbol{a}_t, \boldsymbol{b}_t, m_t, \boldsymbol{s}_t) f(\bar{\boldsymbol{y}}_t, \boldsymbol{a}_t, \boldsymbol{b}_t, m_t | \underline{\boldsymbol{y}}_t, \boldsymbol{s}_t)$$

$$= f(\boldsymbol{z}_t | \boldsymbol{y}_t, \boldsymbol{a}_t, m_t, \boldsymbol{s}_t) f(\bar{\boldsymbol{y}}_t, \boldsymbol{a}_t, \boldsymbol{b}_t, m_t | \underline{\boldsymbol{y}}_t, \boldsymbol{s}_t). \quad (33)$$

Eventually, by inserting (33) into (31) and (31) into (32), we obtain the factorization in (11).

REFERENCES

[1] S. Mukhopadhyay, C. Wang, M. Patterson, M. Malisoff, and F. Zhang
"Collaborative autonomous surveys in marine environments affected by oil spills," *Cooperative Robots and Sensor Networks*, Anis Koubâa and Abdelmajid Khelil, Eds. Heidelberg, Germany: Springer, 2014, pp. 87–113.

[2] M. Jacobi
"Autonomous inspection of underwater structures,"
in *Robot. Auton. Syst.*, vol. 67, pp. 80–86, May 2015.

[3] M. Ho, S. El-Borgi, D. Patil, and G. Song
"Inspection and monitoring systems subsea pipelines: A review paper,"
Struct. Health Monit., vol. 19, no. 2, pp. 606–645, Mar. 2020.

[4] N. Gracias et al.
"Mapping the Moon: Using a lightweight AUV to survey the site of the 17th century ship 'La Lune' in
Proc. IEEE OCEANS, 2013, pp. 1–8.

[5] S. Sariel, T. Balch, and N. Erdogan
"Naval mine countermeasure missions,"
IEEE Robot. Autom. Mag., vol. 15, no. 1, pp. 45–52, Mar. 2008.

[6] M. R. Dhanak and N. I. Xiros
Handbook of Ocean Engineering. Heidelberg, Germany: Springer, 2016.

[7] J. Melo and A. Matos
"Survey on advances on terrain based navigation for autonomous underwater vehicles,"
Ocean Eng., vol. 139, pp. 250–264, Jul. 2017.

[8] Ø. Hegrenæs and O. Hallingstad
"Model-aided INS with sea current estimation for robust underwater navigation,"
IEEE J. Ocean. Eng., vol. 36, no. 2, pp. 316–337, Apr. 2011.

[9] J. Bao, D. Li, X. Qiao, and T. Rauschenbach
"Integrated navigation for autonomous underwater vehicles in aquaculture: A review,"
Inf. Process. Agric., vol. 7, no. 1, pp. 139–151, Mar. 2020.

[10] P. Liu, B. Wang, Z. Deng, and M. Fu
"INS/DVL/PS tightly coupled underwater navigation method with limited DVL measurements,"
IEEE Sens. J., vol. 18, no. 7, pp. 2994–3002, Apr. 2018.

[11] D. P. William
"Fast target detection in synthetic aperture sonar imagery: A new algorithm and large-scale performance analysis,"
IEEE J. Ocean. Eng., vol. 40, no. 1, pp. 71–92, Jan. 2015.

[12] S. Hożyń
"A review of underwater mine detection and classification in sonar imagery," *Electronics*, vol. 10, no. 23, Jan. 2021.

[13] N. Palomeras, T. Furfaro, D. P. Williams, M. Carreras, and S. Dugelay
"Automatic target recognition for mine countermeasure missions using forward-looking sonar data,"
IEEE J. Ocean. Eng., vol. 47, no. 1, pp. 141–161, Jan. 2022.

[14] A. Mallios, P. Ridao, D. Ribas, and E. Hernández
"Scan matching SLAM in underwater environments,"
Auton. Robot., vol. 36, no. 3, pp. 181–198, Mar. 2014.

[15] N. Fairfield, G. Kantor, D. Jonak, and D. Wettergreen
"Autonomous exploration and mapping of flooded sinkholes,"
Int. J. Robot. Res., vol. 29, no. 6, pp. 748–774, Sep. 2009.

[16] T. Fabbri, F. Di Corato, D. Fenucci, D. Meucci, and A. Caiti
"Multiple target tracking in seabed surveys using the GM-PHD filter,"
in *Proc. IEEE OCEANS*, 2015, pp. 1–6.

[17] J. Melo and S. Dugelay
"AUV mapping of underwater targets,"
in *Proc. IEEE OCEANS*, 2019, pp. 1–6.

[18] M. Fröhle, C. Lindberg, K. Granström, and H. Wymeersch
"Multisensor Poisson multi-Bernoulli filter for joint target-sensor state tracking,"
IEEE Trans. Intell. Veh., vol. 4, no. 4, pp. 609–621, Dec. 2019.

[19] F. R. Kschischang, B. J. Frey, and H.-A. Loeliger
"Factor graphs and the sum-product algorithm,"
IEEE Trans. Inf. Theory, vol. 47, no. 2, pp. 498–519, Feb. 2001.

[20] H.-A. Loeliger, J. Dauwels, J. Hu, S. Korl, L. Ping, and F. R. Kschischang
"The factor graph approach to model-based signal processing,"
Proc. IEEE, vol. 95, no. 6, pp. 1295–1322, Jun. 2007.

[21] J. Melo, D. Gaglione, G. Soldi, P. Braca, and S. Dugelay
"A belief propagation based algorithm for autonomous mapping of underwater targets,"
in *Proc. IEEE OCEANS*, 2020, pp. 1–7.

[22] E. Leitinger, F. Meyer, F. Hlawatsch, K. Witrisal, F. Tufvesson, and M. Z. Win
"A belief propagation algorithm for multipath-based SLAM,"
IEEE Trans. Wireless Commun., vol. 18, no. 12, pp. 5613–5629, Dec. 2019.

[23] M. Brambilla et al.
"Cooperative localization and multitarget tracking in agent networks with the sum-product algorithm,"
IEEE Open J. Signal Process., vol. 3, pp. 169–195, Mar. 2022.

[24] G. Soldi et al.
"Underwater tracking based on the sum-product algorithm enhanced by a neural network detections classifier," *Proc. IEEE Int. Conf. Acoust., Speech Signal Process.*, 2020, pp. 5460–5464.

[25] D. Gaglione, G. Soldi, P. Braca, G. De Magistris, F. Meyer, and F. Hlawatsch
"Classification-aided multitarget tracking using the sum-product algorithm,"
in *IEEE Signal Process. Lett.*, vol. 27, pp. 1710–1714, Sep. 2020.

[26] F. Meyer, T. Kropfreiter, J. L. Williams, R. Lau, F. Hlawatsch, P. Braca, and M. Z. Win
"Message passing algorithms for scalable multitarget tracking,"
Proc. IEEE, vol. 106, no. 2, pp. 221–259, Feb. 2018.

[27] O. Daniell, Y. Petillot, S. Reed, J. Vazquez, and A. Frau
"Reducing false alarms in automated target recognition using local sea-floor characteristics,"
in *Proc. Sensor Signal Process. Defence*, 2014, pp. 1–5.

[28] Y. Bar-Shalom, P. K. Willett, and X. Tian
Tracking and Data Fusion: A Handbook of Algorithms.
Storrs, CT, USA: YBS Publishing, 2011.

[29] H. V. Poor
An Introduction to Signal Detection and Estimation, 2nd ed. New York, NY, USA: Springer, 1994.

[30] J. L. Williams and R. Lau
"Approximate evaluation of marginal association probabilities with belief propagation,"
IEEE Trans. Aerosp. Electron. Syst., vol. 50, no. 4, pp. 2942–2959, Oct. 2014.

[31] F. Meyer, P. Braca, P. Willett, and F. Hlawatsch
"A scalable algorithm for tracking an unknown number of targets using multiple sensors,"
IEEE Trans. Signal Process., vol. 65, no. 13, pp. 3478–3493, Jul. 2017.

[32] T. Li, M. Bolic, and P. M. Djuric
"Resampling methods for particle filtering: Classification, implementation, and strategies,"
IEEE Signal Process. Mag., vol. 32, no. 3, pp. 70–86, May 2015.

[33] M. Roth, G. Hendeby, and F. Gustafsson
"EKF/UKF maneuvering target tracking using coordinated turn models with polar/Cartesian velocity,"
in *Proc. 17th Int. Conf. Inf. Fusion*, 2014, pp. 1–8.

[34] O. J. Woodman
"An introduction to inertial navigation," University of Cambridge, Computer Laboratory, Cambridge, UK, Tech. Rep. UCAM-CL-TR-696, Aug. 2007.

[35] A. S. Rahmathullah, Á. F. García-Fernández, and L. Svensson
"Generalized optimal sub-pattern assignment metric,"
in *Proc. 20th Int. Conf. Inf. Fusion*, 2017, pp. 1–8.

Domenico Gaglione (Member, IEEE) received the B.Sc. and M.Sc. degrees (summa cum laude) in telecommunications engineering from Università degli Studi di Napoli Federico II, Naples, Italy, in 2011 and 2013, respectively, and the Ph.D. degree from the Department of Electronic and Electrical Engineering, University of Strathclyde, Glasgow, U.K., in 2017. He is currently a Research Scientist with NATO STO Centre for Maritime Research and Experimentation (CMRE), La Spezia, Italy. His research interests include statistical signal processing with emphasis on state estimation, data fusion, and multisensor multitarget tracking. He was the recipient of the Best Student Paper Award at the 2015 IEEE International Radar Conference (RadarCon), Arlington, VA, USA, and of the NATO STO Scientific Achievement Award in 2020, as a Member of the Data Knowledge and Operational Effectiveness (DKOE) Research Group at CMRE for Advances in Artificial Intelligence and Information Fusion for Maritime Situational Awareness.

Giovanni Soldi received the master's degree in applied mathematics from the University of Milan, Milan, Italy, in 2011, and the Ph.D. degree in signal processing from Télécom ParisTech, Paris, France, in 2016. Since 2016, he has been a Scientist with the Centre for Maritime Research and Experimentation (CMRE), La Spezia, Italy. His research interests include statistical signal processing with a focus on state estimation, data fusion, and multisensor-multitarget tracking techniques. He was the recipient of the NATO STO Scientific Achievement Award, in 2020, as a Member of the Data Knowledge and Operational Effectiveness (DKOE) Research Group, CMRE for Advances in Artificial Intelligence and Information Fusion for Maritime Situational Awareness.

Paolo Braca (Senior Member, IEEE) received the Laurea degree (summa cum laude) in electronic engineering and the Ph.D. degree (Hons.) in information engineering from the University of Salerno, Fisciano, Italy, in 2006 and 2010, respectively. In 2009, he was a Visiting Scholar with the Department of Electronics and Communication Engineering, University of Connecticut, Storrs, CT, USA. From 2010 to 2011, he was a Postdoctoral Associate with the University of Salerno. In 2011, he joined the NATO STO CMRE, where he is currently a Senior Scientist and a Project Manager. He leaded a number of research projects funded by the European Commission, by the U.S. Office of Naval Research, and other institutions. He conducts research in the general area of statistical signal processing with emphasis on detection and estimation theory, wireless sensor network, multi-agent algorithms, target tracking and data fusion, adaptation and learning over graphs, radar (sonar) signal processing, and machine learning. He has coauthored more than 200 publications in international scientific journals, conference proceedings, and NATO technical reports. He was awarded with the National Scientific Qualification to function as an Associate Professor and a Full Professor with Italian Universities, in 2017 and 2018, respectively. He is with the technical committee of the major international conferences in the field of signal processing and data fusion. He was the recipient of the Best Student Paper Award (first runner-up) at FUSION conference in 2009, and NATO STO Scientific Achievement Award (SAA) 2017 for its contribution to the "Development and Demonstration of Networked Autonomous ASW". His coauthored paper was the recipient of the Best Paper Award (first runner-up) at the SSPD conference in 2019. He was also the recipient of the NATO STO SAA, in 2020, as a Team Leader for the Advances in Artificial Intelligence and Information Fusion for Maritime Situational Awareness. His coauthored article was the recipient of the Young Scientist Contest Award at the Signal Processing Symposium 2021. He is an Associate Editor for the T-AES, ISIF-JAIF, and IET-RSN. In 2017, he was a Lead Guest Editor of the Special Issue "Sonar Multi-Sensor Applications and Techniques" in IET-RSN. He was an Associate Editor for the SP-M, T-SP, and EURASIP-JASP.